Mode Classification in Non-Axisymmetric Structures:

How Nonlinear Can a Cavity Be?

David H. Whittum

In this note we classify the couplings of non-axisymmetric structures to beams, with a scheme like that used to classify beamline magnets. The interest is to quantify the nonlinearities of various modes in a systematic fashion, particularly for high-precision linac devices, where systematic position-readout errors or deflections due to higher-moments are a concern. This work provides a straightforward means to make sense of numerical calculations of [*R/Q*], as we illustrate with the example of a resonant cavity beam-position monitor.

This is the second note in a series on the E158 BPM system.

Outline

1. Introduction

Motivation

Typically in accelerator work, we design a cavity for a single purpose --- acceleration, deflection, or monitoring--- and a standard nomenclature can be applied to characterize the mode coupling in terms of $[R/Q]$ or transverse $[R_\perp/Q]$. Even in the case of higher-modes of such cavities, we are typically interested in the same two quantities. However, for non-axisymmetric structures, modes may contain higher multipole components, with the consequence that a beam may couple in a nonlinear fashion.

In this note we set down a simple formulation categorizing the multipole coefficients required to describe field nonlinearities in an electromagnetic resonator. The results are formally just those one finds in the case of beamline magnets.

The problem that motivated this work is the "linac-style" resonant beam position monitor cavity of interest for the E158 experiment (measurement of A_{LR} at low Q^2 by Møller scattering).[1] This experiment requires precise beam-position monitoring to permit accurate inference of beam-angle on-target. For reasons of cost, it is of interest to make use of existing cavities---rectangular cavities with centered circular beam-ports. For such cavities, and at the 1 μm level in beam position monitoring (or 1% of typical jitter amplitudes), the effect of nonlinear field components on the inferred beam position must be quantified. The classification scheme provided here categorizes certain of the numbers required for the statistical analysis underlying the A_{LR} measurement.

In addition a mode classification such as this informs analysis and design of planar accelerating structures, as for W-Band research at SLAC and Technische Universität Berlin.

Review of $[R/Q]$

Let us review briefly the subject of beam interaction with a lossless cavity.[2] We express the solution for the cavity electric field as a superposition of modes,

$$\vec{E}(\vec{r},t) = \sum_{\lambda} E_{\lambda}(\vec{r}) e_{\lambda}(t),$$

and we employ the convention that modal fields $E_{\lambda}(\vec{r})$ are normalized to unit volume integral. (Units for E_{λ} are $m^{-3/2}$ and units for e_{λ} are $V m^{1/2}$---we'll find some quantities with more attractive units in a moment.) Mode excitation due to a current source term $\vec{J}$ in Maxwell's equations, may be expressed in terms of the overlap integral, evaluated in the frequency domain (Fourier components being denoted by an overtilde),

$$\tilde{J}_{\lambda} = \int d^3\vec{r}\, \tilde{J} \bullet E_{\lambda}.$$

The response of a cavity mode is then given by

$$\left(\omega^2 - \omega_{\lambda}^2\right)\tilde{e}_{\lambda} = -j\omega \frac{1}{\varepsilon_0} \tilde{J}_{\lambda},$$

with ε_0 the electrical permittivity of free-space. To make this more explicit, we consider a ballistic pencil beam, the current density is

$$\vec{J} = \hat{z}\delta^2\left(\vec{r}_{\perp} - \vec{r}_{\perp b}\right) I_b\left(t - \frac{z}{V}\right),$$

where I_b is the beam current waveform, t is the time-coordinate, z is the coordinate displacement down the beamline, and $\vec{r}_{\perp}$ is the coordinate in the transverse plane. The delta function is δ. The beam is assumed to be ballistic, travelling at speed V in the z-direction, centered on the transverse

[1] "A Precision Measurement of the Weak Mixing Angle in Møller Scattering", R. Carr, *et al.*, K.S. Kumar, coordinator, SLAC-Proposal-E-158, Version Dated July 17, 1997.

[2] For a more detailed discussion, see "Introduction to Electrodynamics for Microwave Linear Accelerators", D. Whittum, submitted to *Proceedings of the Joint US-CERN-Japan School, RF Engineering for Particle Accelerators* (World Scientific, to be published). This article can be found at the ARDB Tech. Note web site.

coordinate $\vec{r}_{\perp b}$.

The Fourier transform is

$$\tilde{J}(\vec{r},\omega) = \hat{z}\delta^2(\vec{r}_\perp)\int_{-\infty}^{\infty}\frac{d\omega}{\sqrt{2\pi}}e^{-j\omega t}I_b\left(t-\frac{z}{V}\right) = \hat{z}\delta^2(\vec{r}_\perp - \vec{r}_{\perp b})\tilde{I}_b(\omega)e^{-j\omega z/V},$$

and we assume no variation of beam centroid along the beam.The overlap integral that determines the excitation of mode λ is given by

$$\begin{aligned}\tilde{J}_\lambda &= \int d^3\vec{r}\,\tilde{J}\bullet\tilde{E}_\lambda = \int d^3\vec{r}\,\delta^2(\vec{r}_\perp - \vec{r}_{\perp b})\tilde{I}_b(\omega)e^{-j\omega z/V}\hat{z}\bullet\tilde{E}_\lambda \\ &= \tilde{I}_b(\omega)\int_{-\infty}^{+\infty}dz\,E_{z\lambda}(\vec{r}_\perp = \vec{r}_{\perp b}, z)e^{-j\omega z/V} = \tilde{I}_b(\omega)w_\lambda^*(\vec{r}_{\perp b}),\end{aligned}$$

and we abbreviate,

$$\tilde{w}_\lambda(\vec{r}_{\perp b}) = \int_{-\infty}^{+\infty}dz\,E_{z\lambda}(\vec{r}_\perp = \vec{r}_{\perp b}, z)e^{j\omega z/V}. \tag{1}$$

(Units for $\tilde{w}_\lambda$ are $m^{-1/2}$.) Thus Maxwell's equations reduce to

$$\left(\omega^2 - \omega_\lambda^2\right)\tilde{e}_\lambda = -j\omega\frac{1}{\varepsilon_0}\tilde{I}_b(\omega)w_\lambda^*(\vec{r}_{\perp b}).$$

This coefficient $\tilde{w}_\lambda$ we may relate to the more conventional quantity, [*R/Q*], as follows. The voltage drop (or gain) experienced by a test-particle travelling at speed V in the z-direction, and passing z=0 at time $t=t_0$ is

$$V_c(\vec{r}_\perp, t_0) = \int_{-\infty}^{+\infty}dz\,E_z\left(\vec{r}_\perp, z, t_0 + \frac{z}{V}\right).$$

We may express this in terms of the modal decomposition,

$$E_z\left(\vec{r}_\perp, z, t_0 + \frac{z}{V}\right) = \sum_\lambda E_{z\lambda}(\vec{r}_\perp, z)e_\lambda\left(t_0 + \frac{z}{V}\right),$$

corresponding to which we have

$$V_c(\vec{r}_\perp, t_0) = \sum_\lambda V_{c\lambda}(\vec{r}_\perp, t_0),$$

where, in the frequency domain,

$$\tilde{V}_{c\lambda}(\vec{r}_\perp,\omega) = \int_{-\infty}^{\infty} \frac{d\omega}{\sqrt{2\pi}} e^{-j\omega t_0} \tilde{V}_{c\lambda}(\vec{r}_\perp, t_0) = \int_{cavity} dz \int_{-\infty}^{\infty} \frac{d\omega}{\sqrt{2\pi}} e^{-j\omega t_0}\, e_\lambda\left(t_0 + \frac{z}{V}\right) E_{z\lambda}(\vec{r}_\perp, z)$$

$$= \tilde{e}_\lambda(\omega) \int_{-\infty}^{+\infty} dz\, E_{z\lambda}(\vec{r}_\perp, z) e^{j\omega z/V}.$$

Evidently then $\tilde{V}_{c\lambda}(\vec{r}_\perp,\omega) = \tilde{e}_\lambda \tilde{w}_\lambda(\vec{r}_\perp)$, and our cavity equation may be re-expressed in terms of the more meaningful normalizations, $\tilde{V}_c$, $\tilde{I}_b$, according to

$$\left(\omega^2 - \omega_\lambda^2\right) \underbrace{\tilde{V}_{c\lambda}(\vec{r}_\perp,\omega)}_{\tilde{e}_\lambda \tilde{w}_\lambda(\vec{r}_\perp)} = -\frac{j\omega}{\varepsilon_0} \underbrace{\tilde{I}_b \tilde{w}_\lambda^*(\vec{r}_{\perp b}) \tilde{w}_\lambda(\vec{r}_\perp)}_{\tilde{J}_\lambda \tilde{w}_\lambda(\vec{r}_\perp)},$$

or

$$\left(\omega^2 - \omega_\lambda^2\right) \tilde{V}_{c\lambda}(\vec{r}_\perp,\omega) = -j\omega\omega_\lambda \frac{1}{2}\left[\frac{R}{Q}\right]_{\lambda,\vec{r}_\perp,\vec{r}_{\perp b}} \tilde{I}_b$$

with

$$\left[\frac{R}{Q}\right]_{\lambda,\vec{r}_\perp,\vec{r}_{\perp b}} = 2\frac{\tilde{w}_\lambda^*(\vec{r}_{\perp b}) \tilde{w}_\lambda(\vec{r}_\perp)}{\varepsilon_0 \omega_\lambda}.$$

This result may be expressed in the more prescriptive form, evaluated on the beam-axis

$$\left[\frac{R}{Q}\right]_{\lambda,\vec{r}_\perp} = 2\frac{\left|\int_{-\infty}^{+\infty} dz\, E_{z\lambda}(\vec{r}_\perp, z) e^{j\omega_\lambda z/V}\right|^2}{\varepsilon_0 \omega_\lambda \int_{-\infty}^{+\infty} dz \int d^2\vec{r}_\perp \vec{E}_\lambda \bullet \vec{E}_\lambda} = \frac{\left|\tilde{V}_{c\lambda}\right|^2}{\omega_\lambda U},$$

where $\tilde{V}_{c\lambda}$ is evaluated on the beam-axis. In the time-domain, $\tilde{V}_{c\lambda}$ satisifies

$$\left(\frac{d^2}{dt^2} + \omega_\lambda^2\right) V_{c\lambda} = 2k_\lambda \frac{dI_b}{dt},$$

where we have introduced the "loss-factor"

$$k_\lambda = \frac{1}{4}\omega_\lambda \left[\frac{R}{Q}\right]_\lambda.$$

This may be integrated to obtain

$$V_{c\lambda}(t) = 2k_\lambda \int_{-\infty}^{t} dt' \frac{\sin\omega_\lambda(t-t')}{\omega_\lambda} \frac{dI_b}{dt'} = 2k_\lambda \int_{-\infty}^{t} dt' \cos\omega_\lambda(t-t') I_b(t').$$

For a point bunch, the current waveform is a delta-function, $I_b(t') = Q_b \delta(t-t')$, and the induced voltage is $V_{c\lambda}(t) = 2k_\lambda Q_b \cos(\omega_\lambda t) H(t)$, with H the step-function. Work done by the charge is then

$$U_\lambda = \int_{-\infty}^{+\infty} dt\, V_{c\lambda}(\vec{r}_\perp, t) I_b(t) = k_\lambda Q_b^2.$$

Evidently one can determine the mode-excitation by a pencil beam once one knows $[R/Q]$ defined along the beam-orbit.

2. Mode Classification

Let us consider in detail "$[R/Q]$" as defined by

$$\left[\frac{R}{Q}\right]_{\lambda,\vec{r}_\perp} = 2\frac{\left|\tilde{w}_\lambda(\vec{r}_\perp)\right|^2}{\varepsilon_0 \omega_\lambda}, \tag{2}$$

corresponding to a particular choice of beam-axis. This quantity is easily computed for fairly arbitrary geometries, using an electromagnetic field solver. This is to say, a code that solves the eigenvalue problem,

$$\left(\nabla^2 + k_\lambda^2\right)\vec{E}_\lambda = 0$$

with conditions $\hat{n} \times \vec{E}_\lambda = 0$, $\hat{n} \bullet \vec{H}_\lambda = 0$, at conducting boundaries with normal vector $\hat{n}$, and where we define the modal magnetic field according to the normalization $\vec{H}_\lambda = k_\lambda^{-1} \vec{\nabla} \times \vec{E}_\lambda$. Typical output from such a code includes a listing of eigenvalues $k_\lambda = \omega_\lambda / c$, $[R/Q]_\lambda$ for the user-specified beam-axis, and wall Q for each mode, computed according to

$$\frac{1}{Q_{w\lambda}} = \frac{\delta}{2} \int_{surface} dS\, \vec{H}_\lambda^2 = \frac{\delta}{2} \frac{\int_{surface} dS\, \vec{H}_\lambda^2}{\int_{volume} dV\, \vec{H}_\lambda^2},$$

with δ the skin depth of copper evaluated at the mode resonant frequency.

Let us consider a single mode and observe that the transverse dependence of $[R/Q]$ is constrained by Maxwell's equations. Our field integral $\tilde{w}_\lambda$ must satisfy

$$\begin{aligned}\nabla_\perp^2 \tilde{w}_\lambda &= \int_{-\infty}^{+\infty} dz\, e^{j\omega z/V} \nabla_\perp^2 E_{z\lambda}(\vec{r}_\perp, z) = \int_{-\infty}^{+\infty} dz\, e^{j\omega z/V} \left(-\frac{\partial^2}{\partial z^2} - \frac{\omega_0^2}{c^2}\right) E_{z\lambda}(\vec{r}_\perp, z) \\ &= \left(\frac{\omega_0^2}{V^2} - \frac{\omega_0^2}{c^2}\right) \int_{-\infty}^{+\infty} dz\, e^{j\omega z/V} E_{z\lambda}(\vec{r}_\perp, z) = \left(\frac{\omega_0^2}{V^2} - \frac{\omega_0^2}{c^2}\right) \tilde{w}_\lambda,\end{aligned}$$

For a highly relativistic beam (as oppsed to the beam in a klystron, for example), the consequence is that $\tilde{w}_\lambda$ is a harmonic function,

$$\nabla_\perp^2 \tilde{w}_\lambda = 0. \tag{3}$$

This is a strong constraint and we will employ it and related consequences in determining sensitivity to beam transverse coordinates. For example, for a cavity respecting cylindrical symmetry, cavity modes may be categorized by azimuthal harmonic, *m,* in angle θ. Solutions for $\tilde{w}_\lambda$ are then of the form $r^m e^{jm\theta}$. The symmetric mode, with *m*=0, must then have $\tilde{w}_\lambda$ independent of the transverse coordinate. Thus the waveform output by such a mode will be independent of beam position. This result is somewhat counterintuitive when contrasted with the Bessel function dependence of the closed-cavity mode; cancellations occur due to fringe fields near the cavity entrance and exit.

Cavity Impulse or Kick Function

We will shortly embark on a classification of modes, based on the behavior of the function $\tilde{w}_\lambda$ and it will be helpful, for this purpose, to assure ourselves that the function $\tilde{w}_\lambda$ provides a complete description of what a cavity can do to a beam, (in the ballistic approximation). The Lorentz reciprocity theorem then assures us that this quantifies also what the beam can do to the cavity. In addition to the longitudinal impulse determined by the "cavity voltage"

$$V(\vec{r}_\perp, t) = \int_{-\infty}^{+\infty} dz\, E_z\left(\vec{r}_\perp, z, t + \frac{z}{V}\right), \tag{4}$$

the cavity may also provide a transverse kick, determined by the impulse function,

$$\vec{P}_\perp(\vec{r}_\perp, t) = \int_{-\infty}^{+\infty} dz \left\{\frac{1}{V}\vec{E}_\perp + \hat{z}\times\vec{B}_\perp\right\}_{\left(\vec{r}_\perp, z, t+\frac{z}{V}\right)}. \tag{5}$$

The impulse and voltage functions are related as one can show with a bit of algebra. We have

$$\frac{\partial \vec{P}_\perp}{\partial t} = \int_{-\infty}^{+\infty} dz \left\{\frac{1}{V}\frac{\partial \vec{E}_\perp}{\partial t} + \hat{z}\times\frac{\partial \vec{B}_\perp}{\partial t}\right\}_{\left(\vec{r}_\perp, z, t+\frac{z}{V}\right)},$$

and we may evaluate the derivatives using Maxwell's equations,

$$\frac{\partial \vec{B}_\perp}{\partial t} = -\left(\nabla\times\vec{E}\right)_\perp = \hat{x}\left(\frac{\partial E_y}{\partial z} - \frac{\partial E_z}{\partial y}\right) + \hat{y}\left(\frac{\partial E_z}{\partial x} - \frac{\partial E_x}{\partial z}\right).$$

We then employ

$$\frac{\partial V}{\partial x} = \int_{-\infty}^{+\infty} dz \frac{\partial E_z}{\partial x}\left(\vec{r}_\perp, z, t_0 + \frac{z}{V}\right),$$

to obtain

$$\frac{\partial P_x}{\partial t}+\frac{\partial V}{\partial x}=\int_{-\infty}^{+\infty} dz\left\{\frac{1}{V}\frac{\partial E_x}{\partial t}+\frac{\partial E_x}{\partial z}\right\}_{\left(\vec{r}_\perp,z,t\;+\frac{z}{V}\right)}=\int_{-\infty}^{+\infty} dz\,\frac{d}{dz}E_x\left(\vec{r}_\perp,z,t\;+\frac{z}{V}\right)\;=0.$$

Thus in general one has

$$\frac{\partial \vec{P}_\perp}{\partial t}=-\vec{\nabla}_\perp V, \tag{6}$$

the Panofsky-Wenzel theorem. This insures that once we have determined $\tilde{w}_\lambda$, we have determined as well the form kicks may take.

We can take this result a step farther, employing the modal decomposition to express

$$\frac{\partial P_{\perp\lambda}}{\partial t}=-e_\lambda(t)\vec{\nabla}_\perp \tilde{w}_\lambda(\vec{r}_\perp).$$

Employing our result for the modal amplitude, and with choice of basis and z-origin such that w_λ is real, we have

$$\left(\frac{d^2}{dt^2}+\omega_\lambda^2\right)e_\lambda=\frac{1}{\varepsilon_0}\frac{dI_b}{dt}(t)w_\lambda(\vec{r}_{\perp b}),$$

so that

$$\left(\frac{d^2}{dt^2}+\omega_\lambda^2\right)P_{\perp\lambda}=-\frac{1}{\varepsilon_0}I_b(t)w_\lambda(\vec{r}_{\perp b})\vec{\nabla}_\perp w_\lambda(\vec{r}_\perp),$$

or (using $1/\varepsilon_0=cZ_0$),

$$P_{\perp\lambda}(\vec{r}_\perp,t)=-\frac{Z_0}{k_\lambda}\vec{\nabla}_\perp w_\lambda(\vec{r}_\perp)\int_{-\infty}^{t} dt'\sin\omega_\lambda(t-t')I_b(t')w_\lambda(\vec{r}_{\perp b}),$$

with $k_\lambda=\omega_\lambda/c$. The corresponding result for $V_{c\lambda}(\vec{r}_\perp,t)$ is

$$\left(\frac{d^2}{dt^2}+\omega_\lambda^2\right)V_{c\lambda}(\vec{r}_\perp,t)=\frac{1}{\varepsilon_0}\frac{dI_b}{dt}w_\lambda(\vec{r}_{\perp b})\tilde{w}_\lambda(\vec{r}_\perp),$$

or

$$V_{c\lambda}(t)=Z_0c\,w_\lambda(\vec{r}_\perp)\int_{-\infty}^{t} dt'\cos\omega_\lambda(t-t')\,I_b(t')w_\lambda(\vec{r}_{\perp b}).$$

The factor $w_\lambda(\vec{r}_\perp)$ expresses the field line configuration characteristic of the mode, while the factor $I_b(t')w_\lambda(\vec{r}_{\perp b})$ describes the coupling of the beam, on this orbit, to the mode. To make this more explicit, one may consult the mode amplitude,

$$\left(\frac{d^2}{dt^2}+\omega_\lambda^2\right)e_\lambda = Z_0 c\frac{d}{dt}I_b w_\lambda(\vec{r}_{\perp b}),$$

or

$$e_\lambda(t) = Z_0 c\int_{-\infty}^{t} dt' \cos\omega_\lambda(t-t')\, I_b(t') w_\lambda(\vec{r}_{\perp b}).$$

Energy stored in the mode at time t may be expressed as

$$U_\lambda = \frac{1}{2}\int d^3\vec{r}\left\{\varepsilon_0\vec{E}^2+\mu_0\vec{H}^2\right\} \approx \int d^3\vec{r}\,\varepsilon_0\overline{\vec{E}^2} = \frac{1}{Z_0 c}\overline{e_\lambda^2},$$

where $\overline{\cdots}$ denotes an average over one cycle of the oscillation. For a finite beam, one has, after the beam has passed,

$$e_\lambda(t) = Z_0 c\Re\int_{-\infty}^{t} dt' \exp\left[j\omega_\lambda(t-t')\right] I_b(t') w_\lambda(\vec{r}_{\perp b}) = Z_0 c\Re \exp\left[j\omega_\lambda t\right]\int_{beam} dt' \exp\left[-j\omega_\lambda t'\right] I_b(t') w_\lambda(\vec{r}_{\perp b}),$$

so that

$$\overline{e_\lambda^2} = \frac{1}{2}(Z_0 c)^2\left|\int_{beam} dt' \exp\left[-j\omega_\lambda t'\right] I_b(t') w_\lambda(\vec{r}_{\perp b})\right|^2,$$

and

$$U_\lambda = \frac{1}{2}Z_0 c\left|\int_{beam} dt' \exp\left[-j\omega_\lambda t'\right] I_b(t') w_\lambda(\vec{r}_{\perp b})\right|^2.$$

The effective loss-factor is then $k_\lambda = U_\lambda / Q_b^2$, or

$$k_\lambda = \frac{1}{2}Z_0 c\frac{\left|\tilde{I}_b(\omega_\lambda)\right|^2}{\left|\tilde{I}_b(0)\right|^2}\left|\tilde{w}_\lambda(\vec{r}_\perp = \vec{r}_{\perp b})\right|^2,$$

and this we refer to as the "loss-factor with form-factor correction" (units are Ωs^{-1} or VC^{-1}). The form factor is $\left|\tilde{I}_b(\omega_\lambda)/\tilde{I}_b(0)\right|^2$.

Digression: Magnets

For the sake of comparison and illustration, let us digress to consider a localized (discrete) magnet of some kind as depicted in Fig. 1, and let us compute the net kick to an incident electron, under the assumption that electron orbit is ballistic through the magnet.

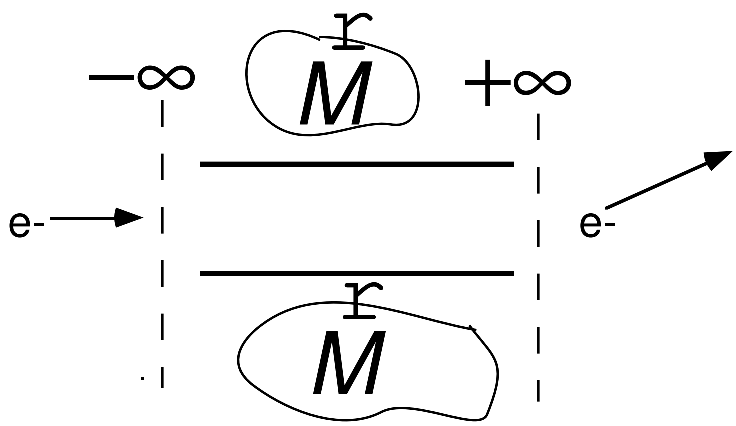

FIGURE 1. An arbitrary discrete magnetic element on the beamline.

We integrate to compute the impulse received by the electron,

$$\frac{d\vec{p}}{dt} = -e\vec{V}\times\vec{B} \Rightarrow \Delta\vec{p} = -e\int_{-\infty}^{+\infty} dt\ \vec{V}\times\vec{B},$$

so that

$$\Delta p_x = -e\int_{-\infty}^{+\infty} dt\ \left(V_y B_z - V_z B_y\right) = -e\int_{-\infty}^{+\infty} ds\ \left(\frac{V_y}{V_z}\frac{\partial\varphi}{\partial s} - \frac{\partial\varphi}{\partial y}\right).$$

(Here we employ s as the coordinate along the beam-orbit, as a matter of convention). Since we are calculating the impulse to first order in the fields (ballistic approximation), V_y may be taken to be constant in the term involving B_z, and in this case integrates to 0. Proceeding in a similar fashion with Δp_y we find that

$$\Delta\vec{p} = -e\hat{s}\times\int_{-\infty}^{+\infty} ds\ \vec{\nabla}\varphi = -e\hat{s}\times\vec{\nabla}_\perp\int_{-\infty}^{+\infty} ds\ \varphi = -e\hat{s}\times\vec{\nabla}_\perp\psi,$$

where,

$$\vec{\nabla}_\perp = \hat{x}\frac{\partial}{\partial x} + \hat{y}\frac{\partial}{\partial y} = \hat{r}\frac{\partial}{\partial r} + \hat{\phi}\frac{1}{r}\frac{\partial}{\partial\phi}, \qquad \psi\left(\vec{r}_\perp\right) = \int_{-\infty}^{+\infty} ds\ \varphi\left(s,\vec{r}_\perp\right).$$

Thus the kinds of kicks we may impart to a paraxial beam at first order in the applied magnetic field are described by the function ψ. Notice that,

$$
\begin{aligned}
\nabla_\perp^2 \psi(\vec{r}_\perp) &= \int_{-\infty}^{+\infty} ds\, \nabla_\perp^2 \varphi(s,\vec{r}_\perp) = \int_{-\infty}^{+\infty} ds \left(\nabla^2 - \frac{\partial^2}{\partial s^2}\right)\varphi(s,\vec{r}_\perp) \\
&= \int_{-\infty}^{+\infty} ds \left(-\frac{\partial^2}{\partial s^2}\right)\varphi(s,\vec{r}_\perp) = -B_s(s,\vec{r}_\perp)\Big|_{-\infty}^{+\infty} = 0,
\end{aligned}
$$

i..e., ψ is a harmonic function. Thus in the region of the beam-pipe, we may express ψ as

$$
\psi(\vec{r}_\perp) = \sum_{m=0}^{\infty} r^m \{a_m \cos(m\phi) + b_m \sin(m\phi)\},
$$

or, in Cartesian coordinates,

$$
\begin{aligned}
\psi = a_0 &+ a_1 x + b_1 y + a_2(x^2 - y^2) + 2b_2 xy + a_3(x^3 - 3xy^2) + b_3(3x^2 y - y^3) \\
&+ a_4(x^4 - 6x^2y^2 + y^4) + 4b_4 xy(x^2 - y^2) \\
&+ a_5(x^5 - 10x^3y^2 + 5xy^4) + b_5(y^5 + 5x^4 y - 10x^2y^3) + \ldots \, .
\end{aligned} \tag{7}
$$

In general, if $\psi(x,y) = \Re f(x + jy)$, with f an analytic function over some region,[3] then ψ satisfies Laplace's equation in that region. Using the binomial theorem,

$$
(a+b)^n = \sum_{k=0}^{n} a^{n-k} b^k \binom{n}{k}, \qquad \binom{n}{k} = \frac{n!}{(n-k)!\,k!},
$$

one can determine the allowed forms for all polynomial terms in the potential ψ.

With the form for ψ in hand, one may continue on to compute the forms the kick to the beam may take, using

$$
\Delta p_x = e\frac{\partial \psi}{\partial y}, \quad \Delta p_y = -e\frac{\partial \psi}{\partial x}, \tag{8}
$$

as determined from the coefficients for the integrated magnetic field,

$$
\begin{aligned}
\int_{-\infty}^{+\infty} ds\, \vec{B}(s,\vec{r}_\perp) = \vec{\nabla}_\perp \psi(\vec{r}_\perp) &= a_1\hat{x} + b_1\hat{y} + 2a_2(x\hat{x} - y\hat{y}) + 2b_2\hat{x}y + 2b_2 x\hat{y} \\
&+3a_3\hat{x}(x^2 - y^2) - 6a_3\hat{y}xy + 6b_3\hat{x}xy + 3b_3\hat{y}(x^2 - y^2)\ldots
\end{aligned}
$$

In this connection, it is conventional to give the terms names as listed in Table 1.

Together with this mathematical description of the moments, one may construct a picture for each term, based on the source terms that would give rise to such a moment. Neglecting fringe effects, the magnet surface is an equipotential contour for ψ. Thus one arrives at the picture of Fig.

[3] Recall that a function f of a complex variable z is said to be *analytic* in a region of the complex plane, if it possess a Taylor series expansion,

$$
f(z) = \sum_{n=0}^{\infty} f_n z^n .
$$

2.

Table 1. Nomenclature for magnet field components. Electron charge is -*e*.

Term	***x*-Kick:** $\Delta p_x / e$	***y*-Kick:** $\Delta p_y / e$	**Nomenclature**
a_1	0	$-a_1$	vertical bend
b_1	b_1	0	horizontal bend
a_2	$-2a_2 y$	$-2a_2 x$	skew quadrupole
b_2	$2b_2 x$	$-2b_2 y$	normal quadrupole
a_3	$-6a_3 xy$	$-3a_3\left(x^2 - y^2\right)$	skew sextupole
b_3	$3b_3\left(x^2 - y^2\right)$	$6b_3 xy$	normal sextupole
a_4	$4a_4\left(y^3 - 3x^2 y\right)$	$-4a_4\left(x^3 - 3xy^2\right)$	skew octupole
b_4	$4b_4\left(x^3 - 3xy^2\right)$	$4b_4\left(y^3 - 3x^2 y\right)$	normal octupole
a_5	$20a_5 xy\left(y^2 - x^2\right)$	$-5a_5\left(x^4 - 6x^2 y^2 + y^4\right)$	skew decapole
b_5	$5b_5\left(x^4 - 6x^2 y^2 + y^4\right)$	$20b_5 xy\left(y^2 - x^2\right)$	normal decapole

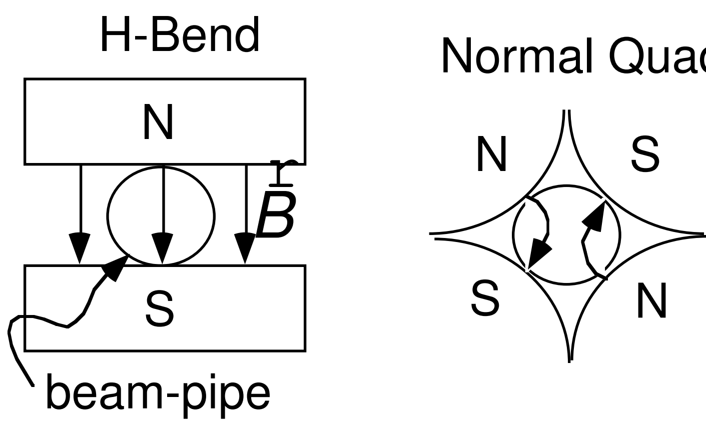

FIGURE 2. The two most commonly employed magnet elements are the horizontal bend (vertical magnetic field), and the "right" or "normal" quadrupole.

Electromagnetic Mode Classification

Next, let us characterize cavity modes in a fashion similar to that employed for magnets. We know that the synchronous field integral

$$\tilde{w}_\lambda\left(\vec{r}_{\perp b}\right) = \int_{-\infty}^{+\infty} dz\, E_{z\lambda}\left(\vec{r}_\perp = \vec{r}_{\perp b}, z\right) e^{j\omega z / V},$$

satisfies

$$\nabla_\perp^2 \tilde{w}_\lambda = 0,$$

and determines the longitudinal and tranverse kicks to the beam,

$$\tilde{V}_{c\lambda}\left(\vec{r}_\perp,\omega\right)=\tilde{e}_\lambda \tilde{w}_\lambda\left(\vec{r}_\perp\right), \qquad \tilde{P}_{\perp c\lambda}=\frac{j}{\omega}\vec{\nabla}_\perp \tilde{V}_{c\lambda}=\frac{j}{\omega}\tilde{e}_\lambda \vec{\nabla}_\perp \tilde{w}_\lambda .$$

As defined $\tilde{w}_\lambda$ need not be real; it is convenient to make $\tilde{w}_\lambda$ real however. We may does this with a choice of the z-coordinate origin, provided we have chosen to employ a real cavity mode basis. To make the analogy with our magnetic formulation more precise, let us employ a function ψ satisfying

$$\vec{\nabla}_\perp \tilde{w}_\lambda=\hat{z}\times\vec{\nabla}_\perp \psi, \qquad \Rightarrow \qquad \frac{\partial\psi}{\partial x}=-\frac{\partial\tilde{w}_\lambda}{\partial y},\quad \frac{\partial\psi}{\partial y}=\frac{\partial\tilde{w}_\lambda}{\partial x}.$$

One can show that ψ is also a harmonic function, $\nabla^2\psi=0$. Analogous to the kick relations for magnets, we have

$$\tilde{P}_{xc\lambda}=\frac{j}{\omega}\tilde{e}_\lambda\frac{\partial\tilde{w}_\lambda}{\partial x}=\frac{j}{\omega}\tilde{e}_\lambda\frac{\partial\psi}{\partial y},\quad \tilde{P}_{yc\lambda}=\frac{j}{\omega}\tilde{e}_\lambda\frac{\partial\tilde{w}_\lambda}{\partial y}=-\frac{j}{\omega}\tilde{e}_\lambda\frac{\partial\psi}{\partial x},$$

or, expressed in the time-domain, in terms of actual momentum impulse, due to mode λ, to an electron passing z=0 at time t,

$$\Delta p_x/e=-P_{xc\lambda}=\left(\int_{-\infty}^{t}dt\,e_\lambda\right)\frac{\partial\psi}{\partial y}, \qquad \Delta p_y/e=-P_{yc\lambda}=-\left(\int_{-\infty}^{t}dt\,e_\lambda\right)\frac{\partial\psi}{\partial x}.$$

This is analogous to Eq. (8), and provides a simple mode categorization. Expressing ψ as in Eq. (7), we may label the terms in a straightforward fashion, as in Table 1.

$$\begin{aligned}\psi=&\underbrace{a_0}_{\text{monopole}}+\underbrace{a_1x}_{\text{vertical dipole}}+\underbrace{b_1y}_{\text{horizontal dipole}}+\underbrace{a_2\left(x^2-y^2\right)}_{\text{skew quad}}+\underbrace{2b_2xy}_{\text{normal quad}}+\underbrace{a_3\left(x^3-3xy^2\right)}_{\text{skew sextupole}}+\underbrace{b_3\left(3x^2y-y^3\right)}_{\text{normal sextupole}}\\ &+\underbrace{a_4\left(x^4-6x^2y^2+y^4\right)}_{\text{skew octupole}}+\underbrace{4b_4xy\left(x^2-y^2\right)}_{\text{normal octupole}}\\ &+\underbrace{a_5\left(x^5-10x^3y^2+5xy^4\right)}_{\text{skew decapole}}+\underbrace{b_5\left(y^5+5x^4y-10x^2y^3\right)}_{\text{normal decapole}}+\ldots\ .\end{aligned}$$

Since the quantity $\tilde{w}_\lambda$ is the thing we will be computing, let us identify the corresponding form for $\tilde{w}_\lambda$,

$$\tilde{w} = \underbrace{b_0}_{monopole} - \underbrace{a_1 y}_{\substack{vertical\\dipole}} + \underbrace{b_1 x}_{\substack{horizontal\\dipole}} - \underbrace{2a_2 xy}_{skew\ quad} + \underbrace{b_2\left(x^2 - y^2\right)}_{normal\ quad} - \underbrace{a_3\left(3x^2 y - y^3\right)}_{skew\ sextupole} + \underbrace{b_3\left(x^3 - 3xy^2\right)}_{normal\ sextupole} +$$
$$- \underbrace{4a_4 xy\left(x^2 - y^2\right)}_{skew\ octupole} + \underbrace{b_4\left(x^4 - 6x^2y^2 + y^4\right)}_{normal\ octupole}$$
$$- \underbrace{a_5\left(y^5 + 5x^4 y - 10x^2 y^3\right)}_{skew\ decapole} + \underbrace{b_5\left(x^5 - 10x^3y^2 + 5xy^4\right)}_{normal\ decapole} + \ldots \ .$$

More concisely,

$$\psi = \Re \sum_{h=0}^{\infty} \left(a_h - jb_h\right)\left(x + jy\right)^h,$$
$$\tilde{w} = -\Im \sum_{h=0}^{\infty} \left(a_h - jb_h\right)\left(x + jy\right)^h = -\Im \sum_{h=0}^{\infty} \left(a_h - jb_h\right) \sum_{p=0}^{h} x^{h-p} y^p j^p \binom{h}{p}.$$

Thus we may examine and categorize modes of a cavity, based on the harmonic properties of $\tilde{w}_\lambda$, In practice, this is assessed by examination of

$$\left[\frac{R}{Q}\right]_{\lambda, \vec{r}_\perp} = 2\frac{\left|\tilde{w}_\lambda\left(\vec{r}_\perp\right)\right|^2}{\varepsilon_0 \omega_\lambda},$$

as computed by an electromagnetic field solver. In general, a mode may contain any or all harmonic components. Use of symmetry can help to delimit the actual terms present. In a cavity with a reflection symmetry, we may delineate modes based on whether $\tilde{w}_\lambda$ is even or odd with respect to reflection. For example, for a cavity with mid-plane symmetry (symmetric upon $y \to -y$) we may expect to find modes odd in *y*,

$$\tilde{w} = -\underbrace{a_1 y}_{\substack{vertical\\dipole}} - \underbrace{2a_2 xy}_{skew\ quad} - \underbrace{a_3 y\left(3x^2 - y^2\right)}_{skew\ sextupole} - \underbrace{4a_4 xy\left(x^2 - y^2\right)}_{skew\ octupole} - \underbrace{a_5 y\left(y^4 + 5x^4 - 10x^2y^2\right)}_{skew\ decapole} + \ldots \ .$$

(odd or skew mode)

and modes even in *y*,

$$\tilde{w} = \underbrace{b_0}_{monopole} + \underbrace{b_1 x}_{\substack{horizontal\\dipole}} + \underbrace{b_2\left(x^2 - y^2\right)}_{normal\ quad} + \underbrace{b_3 x\left(x^2 - 3y^2\right)}_{normal\ sextupole} + + \underbrace{b_4\left(x^4 - 6x^2y^2 + y^4\right)}_{normal\ octupole} + \underbrace{b_5 x\left(x^4 - 10x^2y^2 + 5y^4\right)}_{normal\ decapole} + \ldots \ .$$

(even or normal mode)

***Cavity with Reflection Symmetry in* x & y**

For purposes of the next section, we will be interested in a cavity with reflection symmetry in *x* and *y*. These symmetries strongly constrain the modal integral. Choices are

$$\tilde{w}_{odd-odd} = -\underbrace{2a_2 xy}_{skew\ quad} - \underbrace{4a_4 xy\left(x^2 - y^2\right)}_{skew\ octupole} + O\left(r_\perp^6\right)\ldots \ ,$$
$$\tilde{w}_{even-odd} = -\underbrace{a_1 y}_{\substack{vertical\\dipole}} - \underbrace{a_3 y\left(3x^2 - y^2\right)}_{skew\ sextupole} - \underbrace{a_5 y\left(y^4 + 5x^4 - 10x^2y^2\right)}_{skew\ decapole} + O\left(r_\perp^7\right)\ldots \ ,$$

$$\tilde{w}_{odd-even} = \underbrace{b_1 x}_{\substack{horizontal\\dipole}} + \underbrace{b_3 x\left(x^2 - 3y^2\right)}_{normal\ sextupole} + \underbrace{b_5 x\left(x^4 - 10x^2y^2 + 5y^4\right)}_{normal\ decapole} + O\left(r_\perp^7\right)\ldots ,$$

$$\tilde{w}_{even-even} = \underbrace{b_0}_{monopole} + \underbrace{b_2\left(x^2 - y^2\right)}_{normal\ quad} + \underbrace{b_4\left(x^4 - 6x^2y^2 + y^4\right)}_{normal\ octupole} + O\left(r_\perp^6\right)\ldots .$$

We will categorize modes based on their lowest order behavior,

$\tilde{w} \propto 1 \Rightarrow$ monopole,

$\tilde{w} \propto y \Rightarrow$ vertical dipole, $\qquad \tilde{w} \propto x \Rightarrow$ horizontal dipole.

$\tilde{w} \propto \left(x^2 - y^2\right) \Rightarrow$ normal quad, $\qquad \tilde{w} \propto xy \Rightarrow$ skew quad.

The behavior of each kind of mode may characterized, at this order, as follows.

Monopole Modes

For monopole modes we have

$$\tilde{w}_{even-even} = b_0\left\{1 + \frac{b_2}{b_0}\left(x^2 - y^2\right) + \frac{b_4}{b_0}\left(x^4 - 6x^2y^2 + y^4\right) + O\left(r_\perp^6\right)\ldots\right\}.$$

(monopole mode with residual normal quad, normal octupole)

The coupling parameter b_0 may be quantified more colloquially simply by the [*R/Q*] evaluated on-axis,

$$\lim_{\vec{r}_\perp \to 0}\left[\frac{R}{Q}\right]_{monopole} = 2\frac{\left|\tilde{w}_\lambda(\vec{r}_\perp = 0)\right|^2}{\varepsilon_0 \omega_\lambda} = Z_0 2k_\lambda^{-1} b_0^2 .$$

The normal quadrupole coefficient $\varepsilon_{NQ} = b_2 / b_0$ may be evaluated from a calculation of [*R/Q*] on one or several off-axis orbits, chosen away from the lines *x*=±*y*. In practice we will evaluate [*R/Q*] on a grid of points, and thus allow the electromagnetic solver to tell us what kind of mode components we have. We can satisfy ourselves that the result is reasonable by identifying the corresponding mode of the closed cavity, and checking the zeroth-order [*R/Q*] with the value obtained analytically for the closed cavity. This is to say that we are primarily employing the solver to compute ε_{NQ} (as well as perturbed mode frequency in the presence of ports).

Dipole Modes

For vertical dipole modes we have

$$\tilde{w}_{even-odd} = -a_1 y\left\{1 + \frac{a_3}{a_1}\left(3x^2 - y^2\right) + \frac{a_5}{a_1}\left(y^4 + 5x^4 - 10x^2y^2\right) + O\left(r_\perp^6\right)\ldots\right\},$$

(vertical dipole mode with residual skew sextupole, skew decapole)

where the coupling parameter a_1 may be quantified more colloquially simply by the $[R_\perp / Q] = [R/Q]/y^2$, evaluated from $[R/Q]$ at a finite *y*-displacement,

$$\lim_{r_\perp \to 0}\left[\frac{R}{Q}\right]_{y-dipole} = Z_0 2k_\lambda^{-1} a_1^2 y^2 \qquad (y\text{-dipole})$$

The skew sextupole component $\varepsilon_{SS} = a_3 / a_1$, the skew decapole component $\varepsilon_{SD} = a_5 / a_1$ and higher coefficients require one or several additional off-axis evaluations. The procedure is similar for horizontal dipole modes,

$$\tilde{w}_{odd-even} = b_1 x\left\{1 + \frac{b_3}{b_1}\left(x^2 - 3y^2\right) + \frac{b_5}{b_1}\left(x^4 - 10x^2y^2 + 5y^4\right) + O\left(r_\perp^6\right)\ldots\right\}.$$

(horizontal dipole mode with residual normal sextupole, normal decapole)

We have at lowest order,

$$\lim_{r_\perp \to 0}\left[\frac{R}{Q}\right]_{x-dipole} = Z_0 2k_\lambda^{-1} b_1^2 x^2, \qquad (\text{perfect } x\text{-dipole})$$

Nonlinearity is characterized by the normal sextupole coefficient $\varepsilon_{NS} = b_3 / b_1$, and the normal decapole coefficient, $\varepsilon_{ND} = b_5 / b_1$, and higher order terms.

Quadrupole Modes

For normal quads,

$$\tilde{w}_{even-even} = b_2\left(x^2 - y^2\right) + b_4\left(x^4 - 6x^2y^2 + y^4\right) + O\left(r_\perp^6\right)\ldots, \qquad (\text{normal quad mode})$$

and nonlinearities are characterized by the normal octupole coefficient $\varepsilon_{NO} = b_4 / b_2$. Similarly for skew quads,

$$\tilde{w}_{odd-odd} = -2a_2 xy - 4a_4 xy\left(x^2 - y^2\right) + O\left(r_\perp^6\right)\ldots, \qquad (\text{skew quad mode})$$

and nonlinearities are characterized by the skew octupole coefficient $\varepsilon_{SO} = a_4 / a_2$.

At this order, one could be concerned too with leading order sextupole modes. However, for the example of the next section, these are sufficiently far-removed in frequency to be of less concern.

One can go a step further with this, and ask, of the modes allowed by symmetry, which are present? Does a cavity have a normal quad mode? When the cavity beam-ports respect the symmetry of the cavity proper, one may infer the form of the kick function from the symmetry of the corresponding mode of the unperturbed (closed) cavity. In this way, one may map TM modes of the closed cavity to the “TM-like” modes of the cavity with beam ports. To enumerate all modes however, one must consider as well the TE modes of the closed cavity, for with the addition of beam-ports, these modes will develop longitudinal fringe electric fields that can couple to the beam.

Let us be more specific. We consider the cavity depicted in cartoon-fashion in Fig. 3, and we sketch in Fig. 4, the possible modes at leading order. We can make some estimates concerning the modes, based on nominal dimensions *a*, *b*, and *d*. We suppose the *x*-dimension *a* is larger than the *y*-dimension *d*.

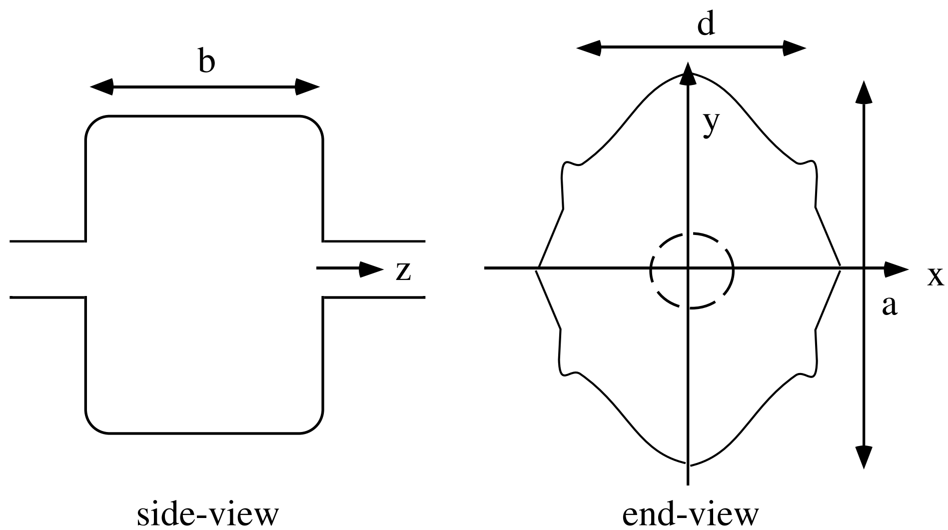

FIGURE 3. Side-view and end-view of a cavity formed by terminated guide with uniform cross-section, and subsequently perturbed by beam-ports.

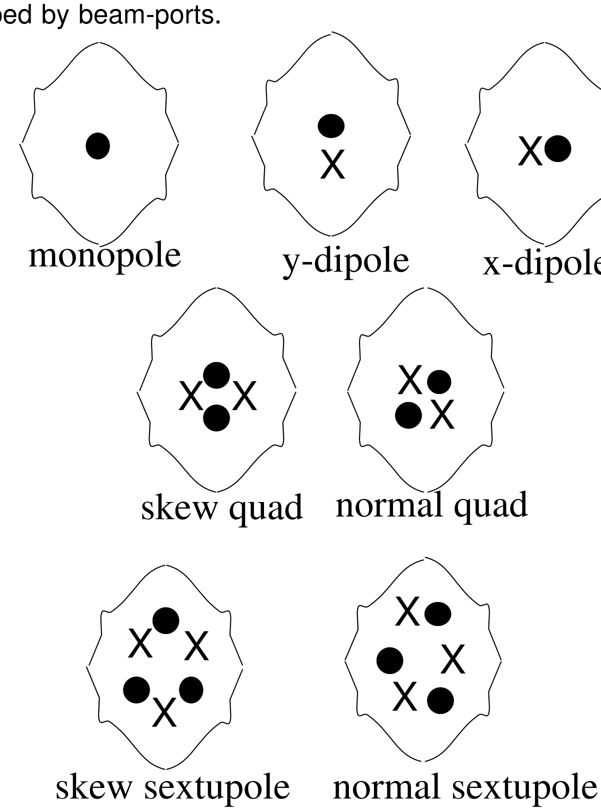

FIGURE 4. Integrated longitudinal electric field (synhronous integral) configuration for various modes of the cavity of Fig. 3, viewed end-on.

To construct the modes, we may attempt to match actual electric field lines to the integrated field pattern depicted in Fig. 4. Characteristic wave numbers are of order $\beta_x \approx \pi / a$ and $\beta_y \approx \pi / d$ for modes derived from the TM analogs for the closed pillbox. For TE modes one has in addition $\beta_z \approx \pi / b$, and these should be accounted for, since longitudinal components develop due to the ports. One expects a monopole mode derived from the lowest TM mode of the cavity, with frequency $f \approx c\beta_0/2\pi$, where $\beta_0 \approx \sqrt{\beta_x^2+\beta_y^2}$. Next one expects to find two dipole modes, an x-dipole at $\beta_0 \approx \sqrt{(2\beta_x)^2+\beta_y^2}$, and a y-dipole at $\beta_0 \approx \sqrt{\beta_x^2+(2\beta_y)^2}$. The next modes would be TE-derived dipole modes (or hybrid modes), corresponding to $\beta_0 \approx \sqrt{\beta_x^2+\beta_z^2}$ (y-dipole, hybrid) and $\beta_0 \approx \sqrt{\beta_y^2+\beta_z^2}$ (x-dipole, hybrid). Clearly, where the modes actually fall in frequency depends on b. For large b, the hybrid dipole modes come first, for very short b, they are preceded by still other modes.

3. Linac-Style Position Cavity

The so-called "linac-style" or "in-line" resonant beam position monitor cavity has been described by Brunet, *et al.*.[4] A summary of the (now mostly decommissioned) beam-position monitor system as whole can be found in the "Blue Book".[5] The cavity of interest is the "position-cavity", depicted in Fig. 5. A number of different kinds of pickup were considered. Evidently there was some interest in having a square cavity with four outputs; difficulty in tuning is reported (!). The arrangment chosen is ideal, except for the asymmetric output coupling (see other modes below). In one cavity, only one mode is resonantly excited, and cross-talk between two beam degrees of freedom is less of a concern. Which degree of freedom one is looking at depends on the alignment during installation. Aperture of 0.8" was chosen to be slightly larger than the accelerator structure aperture.

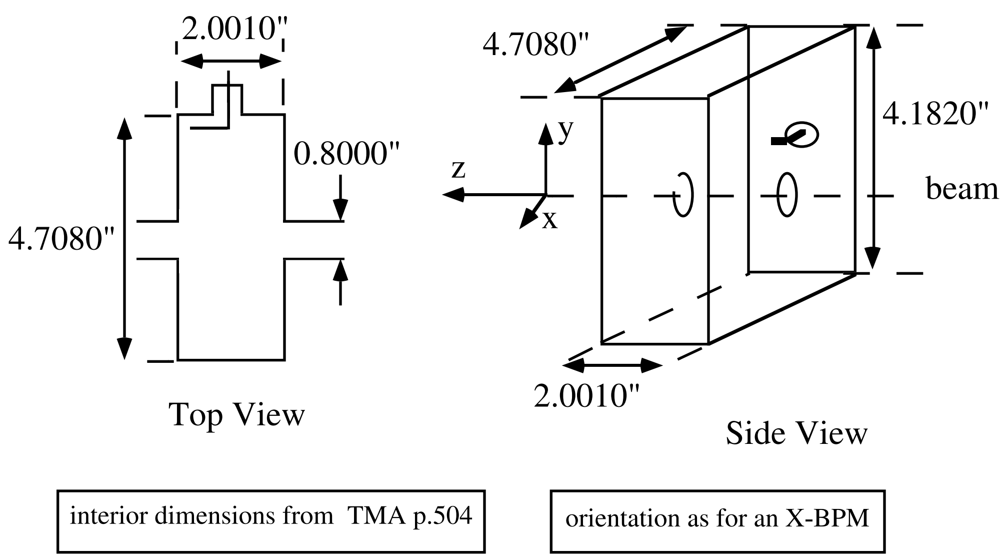

FIGURE 5. Major interior (electrical)dimensions for one linac-style position cavity.

To appreciate the fields and coupling of the position cavity, let us first analyze the cavity without beam-ports, as in Fig. 6. For beam and cavity-axis perfectly parallel, the beam couples only to TM modes of the pillbox (those with an axial electric field). The lowest frequency modes are the TMmn0 modes (no longitudinal variation in axial electric field), with field components

[4] P. Brunet, J. Dobson, M. J. Lee, and C. B. Williams, "Microwave Beam Position Monitors", SLAC TN 64-45, July, 1964 (available from the SLAC Library).

[5] *The Two-Mile Accelerator*, R. B. Neal, ed., (W. A. Benjamin, New York, 1968) pp. 500-516.

$$E_z = \tilde{E}_0 \sin(\beta_x x)\sin(\beta_y y),\; Z_0 H_x = j\frac{\beta_y}{\beta_0}\tilde{E}_0 \sin(\beta_x x)\cos(\beta_y y),\, Z_0 H_y = -j\frac{\beta_x}{\beta_0}\tilde{E}_0 \cos(\beta_x x)\sin(\beta_y y),$$

and other components zero. Wavenumbers are

$$\beta_x = \frac{m\pi}{d}, \qquad \beta_y = \frac{n\pi}{a}, \qquad \beta_0 = \sqrt{\beta_x^2 + \beta_y^2}.$$

The resonant angular frequency is $\omega_0 = c\beta_0$. In this notation, the "accelerating mode" or "monopole mode" is TM110, and the first two "position-sensitive" or "dipole modes" are TM210 and TM120. As sketched in Fig. 5, this cavity is intended to function in the TM210 mode as an *x*-sensitive pickup.

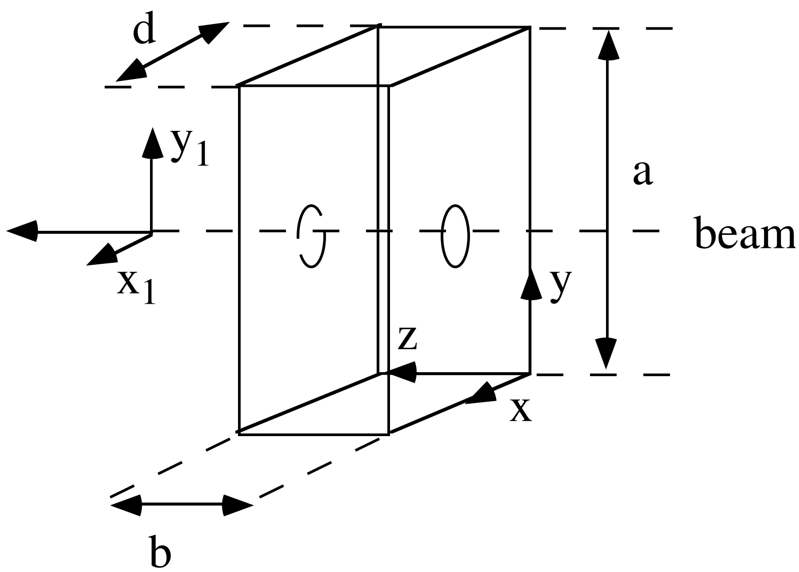

FIGURE 6. We consider a rectangular pillbox; this could be compared to the somewhat more realistic picture of Fig. 5. The pillbox model we will consider does not account for perturbation to the field lines due to the beam ports; however this is thought to be slight based on studies on the Mark IV. For convenience in expressing the fields, we have offset the coordinate notation.

x-*Dipole Mode ("TM210")*

For the desired TM210 mode, paraxially,

$$\tilde{E}_z \approx \tilde{E}_0(-\beta_x x_1)\left(1 - \frac{1}{2}\beta_y^2 y_1^2\right)$$

$$Z_0 H_x \approx j\frac{\beta_y}{\beta_0}\tilde{E}_0(-\beta_x x_1)(-\beta_y y_1), \quad Z_0 H_y \approx -j\frac{\beta_x}{\beta_0}\tilde{E}_0\left(1 - \frac{1}{2}\beta_x^2 x_1^2\right)(-\beta_y y_1),$$

where the coordinates (x_1, y_1) are chosen relative to the beam-axis

$$x = \frac{a}{2} + x_1, \qquad y = \frac{d}{2} + y_1,$$

and $x_1 = y_1 = 0$ for a centered beam. Real fields are obtained from these expressions by multiplying by $\exp(j\omega_0 t)$ and taking the real part.

Stored energy in one such mode is, in terms of the phasor, $\tilde{E}_0$,

$$U = \frac{1}{2}\int dV\left\{\varepsilon_0 \vec{E}^2 + \mu_0 \vec{H}^2\right\} = \int dV\left\langle \varepsilon_0 \vec{E}^2 \right\rangle_{t-avg} = \frac{\varepsilon_0}{2}\int dV\left|\tilde{E}\right|^2 = \frac{\left|\tilde{E}_0\right|^2}{8Z_0 c}V.$$

The cavity volume is $V=abd$. Energy change experienced by a particle entering the cavity at time t_0 on an offset trajectory through (x,y) is

$$\Delta\varepsilon = -e\int_0^b \Re\left\{\tilde{E}_0 e^{j\omega_0(t+z/c)}\sin(\beta_x x)\sin(\beta_y y)\right\}dz = -e\Re\left\{\tilde{V}_c(x,y)e^{j\omega_0 t}\right\},$$

where $\omega_0 = \beta_0 c$ is the mode resonant frequency, and

$$\tilde{V}_c(x,y) = \tilde{E}_0 b\sin(\beta_x x)\sin(\beta_y y).$$

Corresponding to this trajectory, we may define

$$\left[\frac{R}{Q}\right]_{(x,y)} = \frac{\left|\tilde{V}_c(x,y)\right|^2}{\omega U} = Z_0 T^2\left(\frac{8b}{\beta_0 ad}\right)\sin^2(\beta_x x)\sin^2(\beta_y y).$$

We know, from the analysis of the previous section, that the transverse dependence derived here differs when beam ports are added. Nevertheless, this closed-cavity result provides a useful estimate for purposes of checking the leading order value against the output from the field-solver. The transit angle factor is

$$T = \frac{\sin(\theta/2)}{(\theta/2)},$$

where the transit angle $\theta = \beta_0 b$. For the TM210 mode and a paraxial trajectory, we have

$$\left[\frac{R}{Q}\right]_{(a/2+x_1,b/2)} \approx Z_0 T^2\left(\frac{8b}{\beta_0 ad}\right)(\beta_x x_1)^2\left[1-(\beta_y y_1)^2\right],$$

and

$$k_\perp = \frac{1}{x_1^2}\frac{\omega_0}{4}\left[\frac{R}{Q}\right]_{(a/2+x_1,b/2)} \approx (2cZ_0)T^2\left(\frac{\beta_x^2 b}{ad}\right) = \frac{1}{4}\omega_0\left[\frac{R_\perp}{Q}\right].$$

Note that $Z_0 = 4\pi / c$ in cgs units.

Finally the wall Q is of interest. This we may compute from

$$\frac{1}{Q_w} = \frac{\delta}{2} \frac{\int dS \left|\tilde{H}\right|^2}{\int dV \left|\tilde{H}\right|^2}.$$

Consulting the expressions for the fields, one finds

$$\frac{1}{Q_w} = \frac{2\delta}{\beta_0^2} \left(\frac{\beta_x^2}{d} + \frac{\beta_y^2}{a} + \frac{\beta_0^2}{2b} \right),$$

where the skin-depth $\delta \approx 2.1\ \mu\text{m}/\sqrt{f(\text{GHz})} \approx 1.2\ \mu\text{m}$.

Let us evaluate these quantities based on the published dimensions. We have

$$a = 4.1820'' = 10.6223\ \text{cm}, \qquad b = 2.001'' = 5.0825\ \text{cm}, \qquad d = 4.7080'' = 11.9583\ \text{cm},$$

so that

$$\beta_x = \frac{2\pi}{d} = 0.52542\ \text{cm}^{-1}, \qquad \beta_y = \frac{\pi}{a} = 0.29575\ \text{cm}^{-1},\ \beta_0 = \sqrt{\beta_x^2 + \beta_y^2} = 0.60294\ \text{cm}^{-1}.$$

The corresponding frequency is 2.8768 GHz, 20.8 MHz high. Evidently the cutting of the beam port (where magnetic field is large, and electric field small) lowers the frequency by 0.7%. Theoretical wall Q is $Q_w \approx 2.26 \times 10^4$. Transit angle is 199°, corresponding to $T \approx 0.568$. Then

$$\left[\frac{R_\perp}{Q}\right] = Z_0 T^2 \left(\frac{8\beta_x^2 b}{\beta_0 a d} \right) \approx 376.7\,\Omega\,\text{cm}^{-2} \times (0.5679)^2 \times \left(\frac{8 \times (0.52542)^2 \times 5.0825}{0.60294 \times 10.6223 \times 11.9583} \right),$$
$$\approx 17.8\ \Omega\,\text{cm}^{-2}$$

$R_\perp \approx 4.0 \times 10^5\ \Omega / \text{cm}^2$, and loss factor is

$$k_\perp \approx 8\pi T^2 \left(\frac{\beta_x^2 b}{ad} \right) \approx 8.956 \times 10^{-2}\ \text{cm}^{-3} \equiv 8.07 \times 10^{-2}\ V/\text{pC} - \text{cm}^2.$$

Monopole Mode ("TM110")

One concern with an asymmetric output coupling is the inability of the pickup to distinguish, by symmetry, excitation of modes not varying linearly with position. For the position cavity, the concern is the TM110 mode. Unlike the position mode (TM210) this mode has non-zero reading with beam centered. We may refer to it as a "common mode".

With respect to an axis centered in the box, the paraxial fields are for TM110,

$$\tilde{E}_z \approx \tilde{E}_0 \left(1 - \frac{1}{2}\beta_x^2 x_1^2 \right)\left(1 - \frac{1}{2}\beta_y^2 y_1^2 \right),$$

$$Z_0 H_x \approx j\frac{\beta_y}{\beta_0}\tilde{E}_0\left(1-\frac{1}{2}\beta_x^2 x_1^2\right)\left(-\beta_y y_1\right),\ Z_0 H_y \approx -j\frac{\beta_x}{\beta_0}\tilde{E}_0\left(-\beta_x x_1\right)\left(1-\frac{1}{2}\beta_y^2 y_1^2\right),$$

or at lowest order, for a centered beam, simply, a constant axial electric field, and zero magnetic field. Using the prescribed dimensions $a = 10.6223\text{ cm}$, $b = 5.0825\text{ cm}$, $d = 11.9583\text{ cm}$, we compute

$$\beta_x = \frac{\pi}{a} = 0.2958\text{cm}^{-1}, \qquad \beta_y = \frac{\pi}{d} = 0.2627\text{ cm}^{-1}, \qquad \beta_0 = \sqrt{\beta_x^2+\beta_y^2} = 0.3956\text{ cm}^{-1},$$

corresponding to a resonant frequency of $f_M = 1.8875\text{GHz}$. Skin-depth is $\delta \approx 1.6\ \mu\text{m}$, and theoretical wall Q is $Q_w \approx 1.66\times10^4$. Transit angle is 115° and the transit angle factor is $T \approx 0.84$,

$$\left[\frac{R}{Q}\right] = Z_0 T^2\left(\frac{8b}{\beta_0 ad}\right) \approx 215\ \Omega,$$

and loss factor is $k_l \approx 0.64\text{ V/pC}$. Shunt impedance is $R_s = 3.6\,\text{M}\Omega\,(\text{unloaded})$.

y-*Dipole Mode ("TM120")*

In the BPM cavity there is also a *y*-sensitive mode, the TM120 mode, with fields given by

$$\tilde{E}_z \approx \tilde{E}_0\left(1-\frac{1}{2}\beta_x^2 x_1^2\right)\left(-\beta_y y_1\right)$$

$$Z_0 H_x \approx -j\frac{\beta_y}{\beta_0}\tilde{E}_0\left(1-\frac{1}{2}\beta_x^2 x_1^2\right)\left(1-\frac{1}{2}\beta_y^2 y_1^2\right), \quad Z_0 H_y \approx -j\frac{\beta_x}{\beta_0}\tilde{E}_0\left(-\beta_x x_1\right)\left(-\beta_y y_1\right).$$

Due to the symmetry of the TM120 mode, the coupler employed to pickup the TM210 mode does not pickup the TM120 mode. Consequently one is inclined not to be too concerned about the effect of this mode. Nevertheless, let us enumerate the features of this mode, as we did for the TM210 mode. Based on dimensions $a = 4.1820" = 10.6223\text{ cm}$, $b = 2.001" = 5.0825\text{ cm}$, $d = 4.7080" = 11.9583\text{ cm}$, we may compute

$$\beta_x = \frac{\pi}{d} = 0.26271\text{ cm}^{-1}, \qquad \beta_y = \frac{2\pi}{a} = 0.59151\text{ cm}^{-1},$$

the frequency one would compute from this is $\beta_0 = \sqrt{\beta_x^2+\beta_y^2} = 0.64722\text{ cm}^{-1}$, corresponding to 3.088 GHz (232 MHz above the linac frequency). Skin-depth is $\delta \approx 1.2\ \mu\text{m}$ and theoretical wall Q is $Q_w \approx 1.82\times10^4$ Transit angle is 189°, corresponding to $T \approx 0.606$. Loss factor is

$$k_\perp \approx 8\pi T^2\left(\frac{\beta_x^2 b}{ad}\right) \approx 1.294\times10^{-1}\text{ cm}^{-3} \equiv 1.17\times10^{-1}\ V/\text{pC}-\text{cm}^2,$$

about 40% larger than for the TM210 mode, due to the fact that the *y*-dimension of the cavity is smaller. $\left[R_\perp/Q\right] \approx 24.0\ \Omega\text{cm}^{-2}$.

Numerical Modelling of the Position Cavity

As a check of these results, and to accurately determine the higher-order dependence on transverse position, we resort to numerical modelling of the cavity. For this purpose, we employ the code `GdfidL`, described in the Appendix.[6] The numerical geometry is indicated in Fig. 7; due to RAM limitations we employed a mesh factor of `eps`=0.05 rather than `eps`=0.03 as in this figure. (The quantity `eps` is defined in the input file `pos2.M4` given in Appendix A; it determines the step size variable, `STPSZE=eps*zdim`, corresponding to `STPSZE`=0.254127 cm for these runs.) While `GdfidL` has options for specifying the axis for the [*R/Q*] calculation; the version we have does not employ interpolation to compute [*R/Q*], and evidently picks the nearest gridline. The actual axis employed may be computed as follows. The input file permits a translation of the geometry by an amount `(xoff,yoff)` in the transverse plane. The run file `run.x` asks `GdfidL` to compute [*R/Q*] along a line passing through the origin. Meanwhile, `GdfidL` output reports that it failed to do this, and informs the user of the axis actually employed as some value (x_g, y_g) in units of meters. Actual axis is then, in units of cm,

$$(x_a, y_a)[\mathrm{cm}] = 100(x_g, y_g)[\mathrm{m}] - (\hat{x}\mathit{off}, \hat{y}\mathit{off}) \times \mathtt{STPSZE},$$

where we consider translation in units of one step, $\mathtt{xoff} = \hat{x}\mathit{off} \times \mathtt{STPSZE}$, $\mathtt{yoff} = \hat{y}\mathit{off} \times \mathtt{STPSZE}$. Performing repeated GdfidL runs with different values of `(xoff,yoff)`, the transverse dependence of *[R/Q]* may be calculated. For the sake of reference, one complete output file can be found in the Appendix.

Table 2 gives a listing of the first 47 modes; the column marked [*R/Q*]-1 corresponds to (x_a, y_a)=(-0.25,-0.35), while the column marked [*R/Q*]-2 corresponds to (x_a, y_a)= (0.00,0.12) (units are cm). Thus modes with small [*R/Q*]-2 and appreciable [*R/Q*]-1 are modes providing an appreciable response to horizontal position. These quantities are given in units of Ω. The column marked "comment" was filled in following the analysis we describe next.

Analysis of the 1st Monopole Mode (Mode #1, 1893 MHz)

The mode near 1893 MHz is a monopole mode, as one can see by inspecting Table 1. It is just the perturbed version of the TM110 mode of the closed pillbox. Recall that the closed pillbox estimate gave $f_M = 1.8875\,\mathrm{GHz}$, $Q_w \approx 1.66 \times 10^4$, and $[R/Q] \approx 215\,\Omega$. These are quite close to the result of the solver: $Q_w \approx 1.72 \times 10^4$, and $[R/Q] \approx 196\,\Omega$. The higher multipole content of this mode is of some interest in connection with offset correction in the beam-position monitor analysis, as described in TN134. Given the symmetry of the cavity, we expect to find

$$\left[\frac{R}{Q}\right]^{1/2} \approx \left[\frac{R}{Q}\right]_0^{1/2} \left\{1 + \varepsilon_{NQ}(x^2 - y^2) + \varepsilon_{NO}(x^4 - 6x^2y^2 + y^4) + O(r_\perp^6)\mathrm{K}\right\}$$

Analysis of the GdfidL output leads best fit for the normal quadrupole and normal octupole components, $\varepsilon_{NQ} = b_2 / b_0 \approx 6.3 \times 10^{-3}\,\mathrm{cm}^{-2}$, $\varepsilon_{NO} = b_4 / b_0 \approx -5.7 \times 10^{-3}\,\mathrm{cm}^{-2}$. These were obtained by first fitting to the quadrupole component on data corresponding to small offsets, and then fitting the residual with the octupole term. An overlay of the fit and the GdfidL output is seen in Figs. 8(a) and (b). Table 4 compares the `GdfidL` output and the fit; one point disagrees noticeably and

[6] The acronym stands for "Gitter drüber fertig ist die Laube" or "frame up, finished is the shack", emphasizing the importance of the mesh generator to the solver.

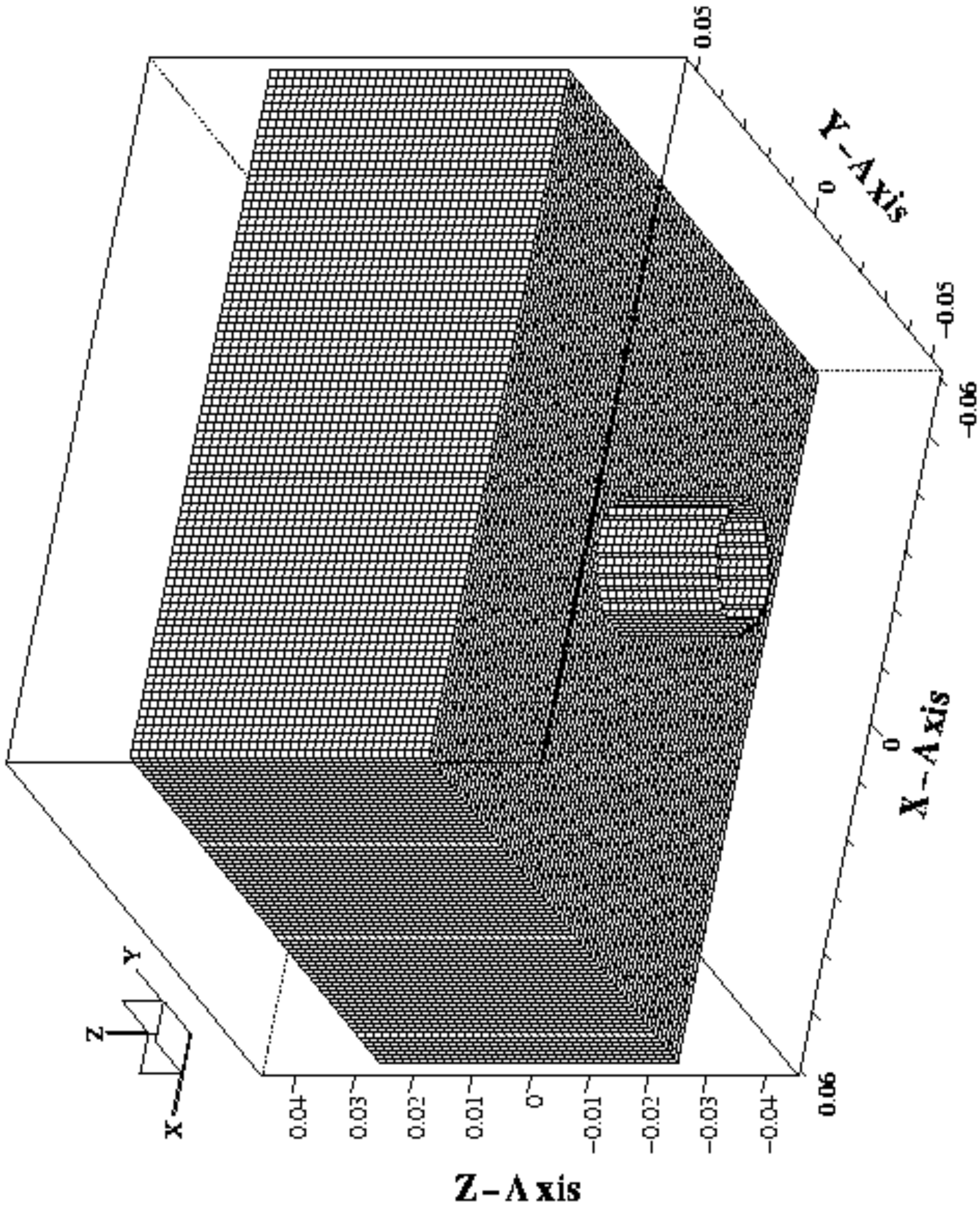

FIGURE 7. Geometry for the GdfidL calculation for a linac-style *x*-cavity.

Table 2. The first 47 modes of the linac position cavity. Units of [*R/Q*] are Ohms.

Mode	f(MHz)	[R/Q]-1	[R/Q]-2	Q_w	comment
1	1892.6	1.96e+02	1.96e+02	1.72e+04	monopole
2	2861.4	1.44e+00	2.83e-10	2.17e+04	x-dipole (design)
3	3071.2	2.87e+00	3.18e-01	2.18e+04	y-dipole
4	3183.6	4.29e-02	4.55e-03	1.90e+04	hybrid y-dipole
5	3247.0	2.87e-02	6.20e-07	1.98e+04	hybrid x-dipole
6	3498.7	2.04e-03	2.15e-03	1.74e+04	
7	3504.6	2.52e+01	2.53e+01	1.54e+04	monopole
8	3771.2	2.64e-02	2.45e-04	2.44e+04	
9	3867.2	8.29e-05	1.87e-05	2.37e+04	
10	4029.3	1.18e+01	1.19e+01	2.42e+04	monopole
11	4077.4	1.01e-01	2.31e-02	2.44e+04	
12	4192.5	3.16e+00	4.33e-01	1.79e+04	
13	4250.5	1.27e-01	3.23e-01	1.97e+04	
14	4417.5	7.18e+00	7.42e+00	2.61e+04	monopole
15	4757.2	8.23e-02	1.19e-02	2.55e+04	
16	4762.1	4.78e-02	5.59e-04	2.90e+04	
17	4993.5	2.18e-01	1.00e-01	2.50e+04	
18	5137.8	1.74e-02	1.90e-04	3.20e+04	
19	5266.6	3.41e+00	2.27e+00	2.55e+04	
20	5673.0	3.85e-01	5.96e-03	2.38e+04	
------5712------------first beam harmonic-------------------------					
21	5793.6	1.93e-02	3.34e-03	3.50e+04	
22	5901.2	3.08e-01	2.67e-02	2.79e+04	
23	5958.6	5.71e-03	6.99e-03	2.64e+04	
24	6355.2	1.85e-01	3.95e-03	3.33e+04	
25	6479.1	8.61e-01	4.31e-02	2.10e+04	
26	6599.6	2.97e-01	4.72e-01	2.58e+04	
27	6897.8	3.75e-02	7.45e-03	3.83e+04	
28	7046.6	5.86e-01	4.52e-01	2.63e+04	
29	7171.3	3.60e-02	5.20e-01	2.78e+04	
30	7508.1	1.33e+00	4.11e-01	2.76e+04	
31	7593.2	7.47e-02	2.88e-02	2.41e+04	
32	7966.4	1.58e-01	1.32e-02	3.00e+04	
33	8108.2	6.84e-01	4.92e-02	1.75e+04	
34	8259.9	9.16e-02	6.32e-03	1.71e+04	
------8568------------second beam harmonic------------------------					
35	8592.2	5.04e-02	1.64e-03	3.27e+04	y-dipole
36	8869.3	3.11e-02	2.26e-03	2.68e+04	
37	9050.3	2.14e-01	1.41e-02	2.33e+04	
38	9217.3	1.65e-01	3.40e-02	3.08e+04	
39	9556.2	6.25e-02	1.04e-02	3.26e+04	
40	9779.5	8.96e-03	2.82e-02	3.14e+04	
41	10172	1.25e-01	1.50e-02	4.28e+04	
42	10349	7.47e-02	1.45e-02	4.73e+04	
43	10747	7.23e-02	3.87e-02	3.43e+04	
44	11165	7.62e-02	1.91e-02	3.55e+04	
------11424-----------third beam harmonic-------------------------					
45	11580	2.21e-02	1.43e-03	4.38e+04	
46	11791	3.61e-02	2.76e-03	3.64e+04	
47	12491	5.64e-02	7.37e-02	4.10e+04	

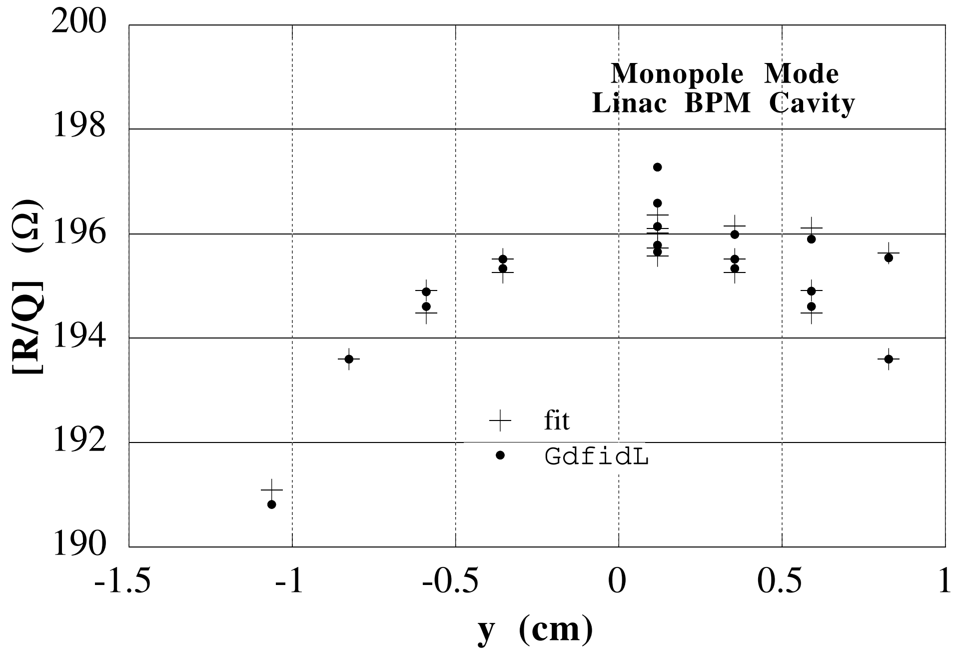

FIGURE 8 (a). Comparison of GdfidL output and the fit for the 1893 MHz monopole mode of the *x*-cavity.

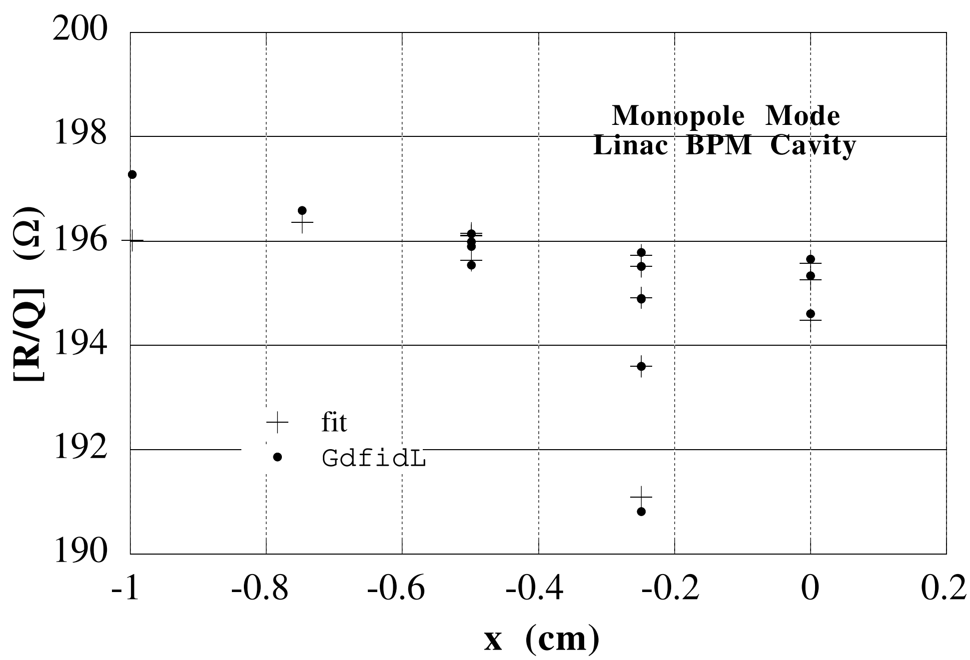

FIGURE 8 (b). Same data as in (a), but plotted versus *x*.

requires further attention.

Table 3. Result of a grid scan for [*R/Q*] for the monopole mode.

x_a (cm)	y_a (cm)	[*R/Q*] (Ω)	Fit
-0.2491	-0.3541	195.51	195.51
-0.2491	-0.5901	194.89	194.91
-0.2491	-0.8262	193.60	193.60
-0.2491	-1.0622	190.82	191.10
-0.2491	0.3541	195.51	195.51
-0.2491	0.5901	194.90	194.91
-0.2491	0.8262	193.60	193.60
-0.2491	0.8262	193.60	193.60
-0.4983	0.8262	195.54	195.63
-0.4983	0.5901	195.90	196.11
-0.4983	0.3541	195.99	196.16
0.0000	0.1180	195.65	195.57
-0.2491	0.1180	195.78	195.73
-0.4983	0.1180	196.14	196.09
-0.7474	0.1180	196.59	196.36
-0.9965	0.1180	197.27	196.01
0.0000	-0.3541	195.33	195.26
0.0000	0.3541	195.33	195.26
0.0000	0.5901	194.61	194.48
0.0000	-0.5901	194.60	194.48

Analysis of the x-Dipole Mode (Mode #2, 2861 MHz)

The mode near 2856 MHz is the intended operating mode for the cavity. A survey of [*R/Q*] over a range of (x_a, y_a) determines the variation listed in column 3 of Table 4.

This mode falls into the category of an "odd in x, even in y" mode and so the synchronous integral must take the form

$$\tilde{w}_{odd-even} = b_1 x \left\{ 1 + \underbrace{\frac{b_3}{b_1}\left(x^2 - 3y^2\right)}_{normal\ sextupole} + \underbrace{\frac{b_5}{b_1}\left(x^4 - 10x^2y^2 + 5y^4\right)}_{normal\ dodecapole} + O\left(r_\perp^6\right) \ldots \right\}.$$

In terms of the variables

$$u_S = x^2 - 3y^2,\ u_D = x^4 - 10x^2y^2 + 5y^4,$$

we may then expect to find a good fit of the form

$$\left[\frac{R}{Q}\right]^{1/2} \approx |x| \left[\frac{R_\perp}{Q}\right]^{1/2} \left(1 + \varepsilon_{NS} u_S + \varepsilon_{ND} u_D\right).$$

with normal sextupole coefficient $\varepsilon_{NS} = b_3 / b_1$, and the normal dodecapole coefficient, $\varepsilon_{ND} = b_5 / b_1$. To determine the fit coefficients, we first removed points corresponding to very small or zero x-values. We then considered only those points on the grid correspdonding to small values of u_D, and performed a least-squares fit versus u_S. We then restored values corresponding to large u_D, and performed a linear fit on the residual versus u_D. The result is

$$\left[\frac{R_\perp}{Q}\right] \approx 23.2\,\Omega\mathrm{cm}^{-2}, \quad \varepsilon_{NS} = -4.2\times10^{-3}\mathrm{cm}^{-2}, \qquad\qquad \varepsilon_D = -4.4\times10^{-3}\mathrm{cm}^{-4}.$$

and numerical values are listed in column 4 of Table 3. Results are compared in Fig. 9. Values agree to three digits in most cases, except for offsets approaching 1 cm, where they agree to two digits. In practical terms, for a 1 mm offset these terms amount to a correction at the level of 100 ppm in beam-induced voltage, and will be completely negligible. Given that the beam pipe radius is 1 cm, the maximum correction one could produce (if one were trying) would be at the level of 1% in voltage, at the cost of scraping beam in the aperture.

Table 4. Result of a grid scan for [*R/Q*] for the design mode.

x_a (cm)	y_a (cm)	[*R/Q*] (Ω)	Fit
-0.2491	-0.3541	1.440	1.4458
-0.2491	-0.5901	1.450	1.4490
-0.2491	-0.8262	1.440	1.4421
-0.2491	-1.0622	1.410	1.4111
-0.2491	0.3541	1.440	1.4458
-0.2491	0.5901	1.450	1.4490
-0.2491	0.8262	1.440	1.4421
-0.2491	0.8262	1.440	1.4421
-0.4983	0.8262	5.840	5.8205
-0.4983	0.5901	5.810	5.8169
-0.4983	0.3541	5.770	5.7831
0.0000	0.1180	0.000	0.0000
-0.2491	0.1180	1.440	1.4419
-0.4983	0.1180	5.760	5.7569
-0.7474	0.1180	12.930	12.8958
-0.9965	0.1180	22.950	22.7191
0.0000	-0.3541	0.000	0.0000
0.0000	0.3541	0.000	0.0000
0.0000	0.5901	0.000	0.0000
0.0000	-0.5901	0.000	0.0000

The solver results, $\left[R_\perp/Q\right] \approx 23.2\,\Omega\mathrm{cm}^{-2}$, and $Q_w \approx 2.17\times10^4$ can be compared to the closed-pillbox values $\left[R_\perp/Q\right] \approx 17.8\,\Omega\,\mathrm{cm}^{-2}$, $Q_w \approx 1.82\times10^4$. [It is actually somewhat puzzling that these two results aren't closer, and we are still looking into this. Runs performed with an improved mesh will be included in revision.]

Modes 3,4 and 35

The 3017 MHz mode (mode #3) is a y-dipole mode with $\left[R_\perp/Q\right] \approx 22.8\,\Omega\ \mathrm{cm}^{-2}$. Mode #4, the 3184 MHz mode is also a y-dipole mode, a hybrid derived from the lowest TE mode of the closed pillbox, TE101. For reference we note the closed pillbox estimates for this mode, corresponding to

$$\beta_x = \frac{\pi}{d} = 0.26271 \text{ cm}^{-1}, \qquad \beta_y = 0, \qquad \beta_z = \frac{\pi}{b} = 0.61812 \text{ cm}^{-1},$$

or $\beta_0 = \sqrt{\beta_x^2 + \beta_z^2} = 0.67163 \text{ cm}^{-1}$, and a frequency of 3.205 GHz. This mode has a vertical electric field developing a longitudinal component due to the beam-ports, with a resulting odd symmetry in y, and even symmetry in x. It has a low $[R_\perp / Q] \approx 0.3\ \Omega\ \text{cm}^{-2}$, as does the 3247 MHz x-dipole hybrid with $[R_\perp / Q] \approx 0.4\ \Omega\ \text{cm}^{-2}$, derived from the TE011 mode. Other features to note: the common mode signal will include a sum over all monopole modes. However in the resonant mode of operation, these suffer cancellations; for future work, we simply employ estimates based on mode #1 to bound such effects.

One additional mode is noteworthy in that it is located rather close to a beam harmonic. This is mode #35, at 8592 MHz, a y-dipole mode with $[R_\perp / Q] \approx 0.7\ \Omega \text{cm}^{-2}$. If the mode of the actual cavity (as opposed to our numerical model) were in fact 24 MHz away from the 3×2856 MHz = 8568 MHz beam harmonic, this would be no cause for concern. However, at the 24 MHz level, one would prefer to check the actual cavity (with coupler, under vacuum, and at temperature) to see where the mode lies.

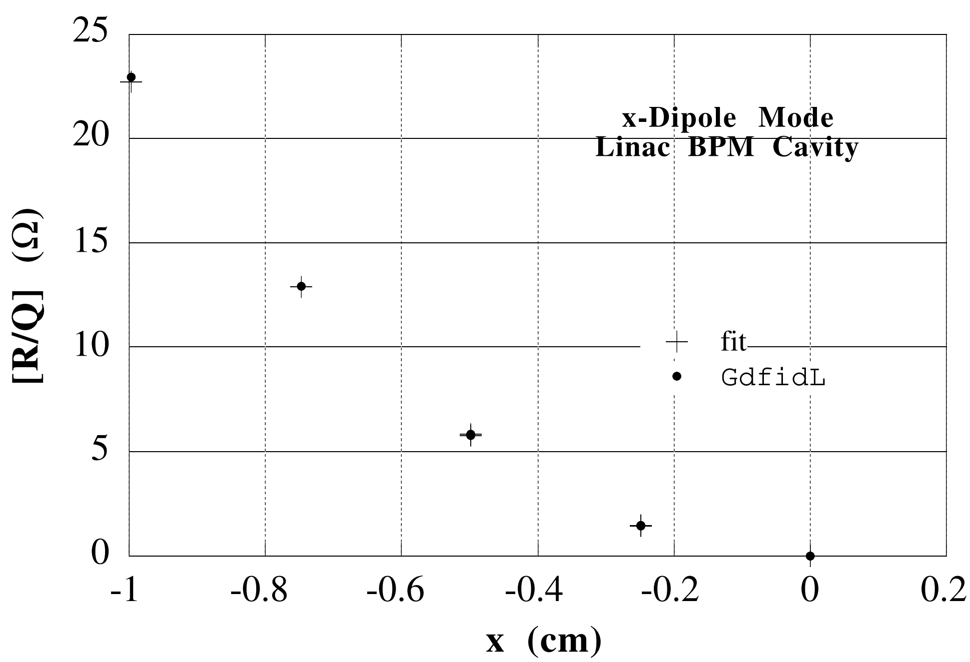

FIGURE 9. Comparison of the fit and the GdfidL calculation for the design mode of the linac-style *x*-cavity.

4. Summary

The typical code listing of modes, does not come with a label indicating what exactly to make of $[R/Q]$. For example, for the TM110 mode of a right circular cylinder, the result is zero for a centered beam-axis. "Zero" is not very informative, and it is conventional for such a case to evalute $[R/Q]$ at a transverse displacement a, and to quote $[R_\perp / Q] = [R/Q]_a / a^2$. For an asymmetric structure, the variation of $[R/Q]$ with transverse position has a fair variety to it, and is amenable to classification much as linac magnets are. In the case of a magnet and, for accurate beam-optics work, one is interested to know not only the dipole field on-axis, and the quadrupole gradient, but higher-moments as well. In the case of an electromagnetic structure one is likewise interested in these higher moments, when high precision is required.

We have provided a simple multipole categorization scheme for modes of an asymmetric resonator, a scheme that provides helpful tools for extracting nonlinearities from electromagnetic solvers. We have applied this analysis to an example of current interest, the “linac-style” position cavity.

Appendix: Electromagnetic Computations with GdfidL

The code GdfidL is a finite difference program for calculation of electromagnetic fields in resonant structures. It has been thoroughly described and documented by its author, Warner Bruns and is available on the SLAC Unix system, complete with a user manual, and examples for getting started.[7] On the SLAC Unix system, GdfidL is best run from the machine "wilson", employing a directory in u5. The calculation is initiated with the line command

```
>run.x
```

referring to the script

```
# File=run.x
#     SET VIEWING ANGLE
#
GDFIDL_EYEPOS="eyepos.x=0.05. eyepos.y=0.1 eyepos.z=-.05"
export GDFIDL_EYEPOS
#
#     CONFIGURED TO RUN GDFIDL FOR THE E158/LINAC STYLE
#     POSITION SENSITIVE CAVITY....SEE ARDB TN #134
#
 M4 -DISHOW=0 < pos2.M4 > plain_numbers
 gdfidl \
      -RoQ \
      -plotopts=" -nopixmap -Phpae1a -colorps" \
      -shut_up \
      < plain_numbers | tee out
```

The program M4 preprocesses the input file pos2.M4,

```
#-----------------------------------------------------------------------
# File= pos2.M4
#       The input file for the LINAC STYLE CAVITY BPM
#     2856 MHz TM210, rectangular
#     REF: ARDB TN134
# Date= 27 October 1997
#-----------------------------------------------------------------------
# ******************************************************************
# --- definition of symbols for material numbers and for "infinity".
# ******************************************************************
define(VAC,0)                #
define(EL,1) define(MAG,2)   #
define(INF, 1000)      #
define(LARGE,1.E20)          #
# *******************************************************************
# --- definitions for structure dimensions, in MKS units.
# *******************************************************************
#
```

[7] Warner Bruns, "GdfidL: A Finite Difference Program for Arbitrarily Small Perturbations", TET-Note 95/14 (Technische Universität Berlin, Institut für Theoretische Elektrotechnik, Einsteinufer 17, 10587 Berlin. Prof. Heino Henke's group in Berlin has a web site for this and other technical notes.

```
#     basic dimensions of the cavity in inches
#
define(inch,2.54e-2)            # inch in units of m
define(ydimin,4.1820)           # cav height "a" in inches
define(xdimin,4.7080)           # cav width "d" in inches
define(zdimin,2.0010)           # cav length "b" in inches
define(pipein,0.8000)           # pipe inner diameter in inches
define(freq0,2.856e9)           # design frequency, in Hz
define(band0,eval(2*freq0))     # bandwidth of interest, in Hz
#
#     basic dimensions converted to code units (MKS)
#
define(ydim,eval(ydimin*inch)) # "a" see Fig 2.3 TN
define(xdim,eval(xdimin*inch)) # "d" see Fig 2.3 TN
define(zdim,eval(zdimin*inch)) # "b" see Fig 2.3 TN
define(pipe,eval(pipein*inch)) # pipe diameter
define(rpipe,eval(pipe/2))      # pipe radius
#
#     numerical parameters
#
define(eps,0.05)                # small number, defines mesh, etc
define(zeps,eval(eps*zdim))     # derived from eps, small length
define(zpipe,eval(pipe))        # a depth down the beam pipe
define(xoff,eval(1.*zeps))      # allow offset in x
define(yoff,eval(1.*zeps))      # allow offset in y
#
#     derived parameters for defining cuts
#
define(zwidth,eval(2*zpipe+zdim))# total zwidth of computational volume
define(xwidth,eval(xdim+2*zeps)) # total xwidth         "
define(ywidth,eval(ydim+2*zeps)) # total ywidth         "
define(zmax,eval(zwidth/2))      # max z value, defines volume edge
define(zmin,eval(-zmax))         # min z                "
define(xmax,eval(xoff+xwidth/2)) # max x value,       "
define(xmin,eval(xoff-xwidth/2)) # min x value,       "
define(ymax,eval(yoff+ywidth/2)) # max y value,       "
define(ymin,eval(yoff-ywidth/2)) # min y value,       "
#
#     more derived parameters
#
define(xcr,eval(xoff+xdim/2))  # x-right interior edge of cavity
define(xcl,eval(xoff-xdim/2))  # x-left         "
define(ycr,eval(yoff+ydim/2))  # y-right        "
define(ycl,eval(yoff-ydim/2))  # y-left         "
define(zcr,eval(zdim/2))       # z-right        "
define(zcl,eval(-zcr))         # z-left         "
#
#     more derived parameters, for pipe cut
#
define(lpipe,zwidth)     # length of cylindrical cut for pipe
define(x0p,xoff)         # x-coord, center of left end face
define(y0p,yoff)         # y-coord, center of left end face
define(z0p,zmin)         # z-coord, center of left end face
```

```
define(xnp,0)            # x-component, direction vector for cyl
define(ynp,0)            # y-component,         "
define(znp,1)            # z-component,   "
#
define(STPSZE, zeps)     # the mesh size
#
# *******************************************************************
# --- input block required for the time-domain calculation.
# *******************************************************************
beginFDTD
 monitorfile= ./monitorfile
#
# --- RF power coming in the beam-pipe from negative z
# (from the right in Fig. 2.3)
#
 newport,
  portname= beamin, portplane= zlow,
  portzlow= eval(-LARGE), portzhigh= eval(zmin),
  omodes= 2, nsol= 50, fup= 50e9
#
# --- RF power going out the beam-pipe to positive z
# (to the left in Fig. 2.3)
#
 newport,
  portname= beamout, portplane= zhigh,
  portzlow= eval(zmax), portzhigh= eval(LARGE)
 # same omodes, nsol, fup as before

 eport= beamin,
 emode= 1, eamplitude= 1
 define(FREQ,eval(freq0))
 efrequency= FREQ, ebandwidth= eval(band0)

 tmin= eval(500/FREQ),
 tmax= eval(2000/FREQ)

 tsavefirst= eval(15/FREQ)
 tsavelast= eval(18/FREQ)
 tsavedist= eval(0.25/FREQ)

 dtsafety=0.95

endFDTD
#################
#################
#################
#################

# *******************************************************************
# --- The following block is required for both the frequency
#     and the time domain computation.
# *******************************************************************
beginFDEV # <--- this Keyword markes the block with 10 fixed lines
```

```
'./solution'  # fname
50                      # nsol
25e9                    # fup
STPSZE                  # stpsze
 xmin xmax              # xlow, xhigh
 ymin ymax              # ylow, yhigh
 zmin zmax              # zlow, zhigh
 EL   EL                # xbcl, xbch
 EL   EL                # ybcl, ybch
 MAG  MAG               # zbcl, zbch

#
# --- specify the computational mode
#     ishow=99 generate the mesh; write, display the plotfile and
#     compute.
#     ishow=1 only generate the mesh.
ishow= ISHOW
text()=Linac-Style Position Cavity  #annotation text
text()=Ref. ARDB TN 134 (E158)
# ********************************************************************
# --- Begin to carve the structure ---
# ********************************************************************
#
#           --- fill the whole volume with metal
#
#           example: brick( mat, xl,xh, yl,yh, zl,zh)
#
brick(EL,xmin,xmax,ymin,ymax,zmin,zmax)
#
#           --- create beam pipe
#           example: gccylinder(MAT,RADIUS,LENGTH,X0,Y0,Z0,XN,YN,ZN)
#
gccylinder(VAC,rpipe,lpipe,x0p,y0p,z0p,xnp,ynp,znp)
#
#           --- fill interior cavity volume with VAC
#
brick(VAC,xcl,xcr,ycl,ycr,zcl,zcr)
#
#
#
############## end of file ##############
```

Here is an example output file, "`out`" corresponding the input file, `pos2.M4` given above,

```
trying to allocate 32 MBytes for mesh generation..
 *******************************************************************
 * llf50: cannot find line (x,y)= (    0.0000    ,    0.0000    )     *
 * integrating along       (x,y)= (   49.9535e-06, -999.4898e-06)     *
 *******************************************************************
```

Linac-Style Position Cavity

Ref. ARDB TN 134 (E158)

Boundary conditions:

xboundary= electric, electric

yboundary= electric, electric

zboundary= magnetic, magnetic

The first 2 solutions seem to be static and are not saved.

Shunt-Impedances are calculated at (x,y)= (49.9535e-06, -999.4898e-06) [m]

mode	frequency	accuracy	cont.max	R/Q [Ohm]	Q(all copper)	Q(diff. conduc.'s)	
3	461.7780e+06	1.2	.4547	3.26	6.928e+03	6.929e+03	GdfidL
4	1.8926e+09	.11E-01	.0092	195.51	17.216e+03	17.219e+03	GdfidL
5	2.8614e+09	.24E-02	.0037	1.44	21.665e+03	21.669e+03	GdfidL
6	3.0712e+09	.24E-02	.0178	2.87	21.768e+03	21.772e+03	GdfidL
7	3.1836e+09	.28E-01	.3976	42.90e-03	19.001e+03	19.004e+03	GdfidL
8	3.2470e+09	.27E-01	.1735	28.73e-03	19.809e+03	19.813e+03	GdfidL
9	3.4987e+09	.47E-02	.0321	2.04e-03	17.397e+03	17.400e+03	GdfidL
10	3.5046e+09	.54E-02	.0362	25.25	15.424e+03	15.427e+03	GdfidL
11	3.7712e+09	.89E-02	.0634	26.35e-03	24.401e+03	24.405e+03	GdfidL
12	3.8672e+09	.91E-02	.1076	82.88e-06	23.679e+03	23.684e+03	GdfidL
13	4.0293e+09	.48E-01	.5976	11.84	24.191e+03	24.195e+03	GdfidL
14	4.0774e+09	.15E-01	.2684	101.39e-03	24.411e+03	24.416e+03	GdfidL
15	4.1925e+09	.15	2.7848	3.16	17.933e+03	17.936e+03	GdfidL
16	4.2505e+09	.22	2.7581	126.94e-03	19.684e+03	19.687e+03	GdfidL
17	4.4175e+09	.10E-01	.0672	7.18	26.133e+03	26.138e+03	GdfidL
18	4.7572e+09	.13	.8734	82.26e-03	25.465e+03	25.470e+03	GdfidL
19	4.7621e+09	.90E-01	.9327	47.81e-03	29.042e+03	29.047e+03	GdfidL
20	4.9935e+09	.11	1.2157	218.31e-03	24.995e+03	24.999e+03	GdfidL
21	5.1378e+09	.13E-01	.2390	17.42e-03	32.024e+03	32.030e+03	GdfidL
22	5.2666e+09	.12	.7819	3.41	25.456e+03	25.460e+03	GdfidL
23	5.6730e+09	.45E-01	.3150	384.76e-03	23.753e+03	23.758e+03	GdfidL
24	5.7936e+09	.69E-01	1.6762	19.30e-03	34.962e+03	34.968e+03	GdfidL
25	5.9012e+09	.21	5.8698	307.75e-03	27.903e+03	27.908e+03	GdfidL
26	5.9586e+09	.32E-01	.2389	5.71e-03	26.350e+03	26.355e+03	GdfidL
27	6.3552e+09	.30E-01	.2453	185.24e-03	33.337e+03	33.344e+03	GdfidL
28	6.4791e+09	.63E-01	1.6509	861.04e-03	20.965e+03	20.969e+03	GdfidL
29	6.5996e+09	.16	1.7393	296.75e-03	25.771e+03	25.776e+03	GdfidL
30	6.8978e+09	.40E-01	.4710	37.54e-03	38.286e+03	38.293e+03	GdfidL
31	7.0466e+09	.16	3.8163	586.08e-03	26.274e+03	26.279e+03	GdfidL
32	7.1713e+09	.59E-01	.6221	36.00e-03	27.764e+03	27.769e+03	GdfidL
33	7.5081e+09	.14	1.5929	1.33	27.598e+03	27.602e+03	GdfidL
34	7.5932e+09	.37E-01	.3779	74.67e-03	24.084e+03	24.088e+03	GdfidL
35	7.9664e+09	.99E-01	1.0626	157.69e-03	30.050e+03	30.056e+03	GdfidL
36	8.1082e+09	.34E-01	.9074	684.16e-03	17.498e+03	17.501e+03	GdfidL
37	8.2599e+09	.28E-01	.3519	91.56e-03	17.062e+03	17.065e+03	GdfidL
38	8.5922e+09	.10	1.3774	50.41e-03	32.715e+03	32.721e+03	GdfidL
39	8.8693e+09	.22E-01	.3562	31.09e-03	26.758e+03	26.763e+03	GdfidL
40	9.0503e+09	.36E-01	.9199	214.20e-03	23.346e+03	23.350e+03	GdfidL
41	9.2173e+09	.42E-01	.5726	164.96e-03	30.829e+03	30.834e+03	GdfidL
42	9.5562e+09	.45E-01	.6452	62.52e-03	32.611e+03	32.617e+03	GdfidL
43	9.7795e+09	.61E-01	.7485	8.96e-03	31.437e+03	31.443e+03	GdfidL
44	10.1721e+09	.72E-01	.9443	124.98e-03	42.787e+03	42.795e+03	GdfidL
45	10.3491e+09	.73E-01	.9413	74.69e-03	47.281e+03	47.292e+03	GdfidL
46	10.7472e+09	.55E-01	.6990	72.27e-03	34.305e+03	34.312e+03	GdfidL
47	11.1647e+09	.64E-01	.8465	76.19e-03	35.473e+03	35.479e+03	GdfidL

```
  48  11.5797e+09 .79E-01  1.1054  22.09e-03  43.804e+03  43.813e+03   GdfidL
  49  11.7907e+09 .68E-01   .5687  36.09e-03  36.374e+03  36.381e+03   GdfidL
  50  12.4911e+09 .64E-01   .5534  56.35e-03  41.025e+03  41.032e+03   GdfidL
Start time: 17:24:50
End time  : 17:27:24
date: 06/11/97

filename             :./solutiongdfidl
Processed MFLOPs     :     5.50e+03
CPU-seconds          :   149.07
Resulting MFLOPs/s   :    36.86
Wall clock seconds   :   154.00
Resulting MFLOPs/s   :    35.68
Used Memory (approx.):     35 MByte
nx,ny,nz             :   50   47   37
nx*ny*nz             :   86950
if the prompt does not appear, press Ctrl-C
```